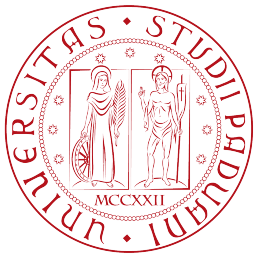

Università degli Studi di Padova

Dipartimento di Fisica e Astronomia "Galileo Galilei"

Master Degree in Astrophysics and Cosmology

Final Dissertation

Model-independent assessment of the compatibility of Supernovae and BAO measurements

Thesis supervisor
Prof. Daniele Bertacca

Thesis co-supervisor
Prof. Marco Raveri

Candidate
Jose Antonio de Jesus Najera Quintana

Academic Year 2023/24

This thesis is dedicated to my parents, Antonio and María, and all my family members who have helped and support me at all times even from another continent. I am deeply grateful of their financial, and emotional support during all these years. I want to give a special mention to my sincere friends, in particular, Carlos, Amanda, Fernando, Isabel, Brisa, Ernesto, Luis, Enrique, Leonardo, Nuria, Fernanda, Sofía, Juan, and Franco, who have been present during all my journey and who have been there for everything that I have needed. Finally, I want to thank the Department of Physics and Astronomy of the University of Padova for providing me a unique opportunity by giving me a full departmental scholarship.

Abstract

In this thesis, we used Type 1a supernovas (SNeIa), calibrated with the local determination of the Hubble constant H_0 using the last result from the SH0ES collaboration, to build a continuous version of the Pantheon+ using Gaussian Process interpolation. This is done in a model-independent way. We use this new catalogue to predict the strong lensing distances from H0LiCOW and the Baryon Acoustic Oscillations distance ratios from DESI to test their compatibility. We found that these predictions using the Pantheon+ catalogue have a perfect agreement with the observational data from H0LiCOW and DESI, showing compatibility at a 1σ C.L. We showed that the agreement between the predicted observations using Pantheon+ and DESI BAO is highly dependent on the calibration of the sound horizon r_d. In particular, using the result from the Planck collaboration, we found that the predicted data would be at 2σ C.L. tension with the DESI BAO data. Our tests give further evidence that there are no significant unaccounted systematic errors that could bias the result from the SH0ES collaboration. Thus, we provide more evidence for the hypothesis that the Hubble constant tension problem has a physical origin.

Contents

Introduction

During the last few years, we have been able to constrain the Cosmological parameters with unprecedented accuracy. In particular, we can now constrain the Hubble constant H_0, which is the parameter measuring the current expansion of the Universe, with 1% accuracy. The most famous of these measurements come from the *Supernova, H0, for the Equation of State of Dark Energy (SH0ES)* collaboration, and the Planck collaboration. The former comes from supernova, and cepheid variables giving a model-independent determination of H_0. On the other hand, the latter comes from the Cosmic Microwave Background (CMB) anisotropies, but it is model-dependent. The model that is used to determine H_0 using CMB anisotropies is the so-called ΛCDM model, the standard model of Cosmology.

The last result of H_0 from the SH0ES collaborations is reported in [1], we will call this *SH0ES 2022*. Meanwhile, the last result from the Planck collaboration is reported in [2] which we will call *Planck 2018*. Interestingly, both results differ at the 5σ confidence level (C.L.). This means that the probability of both measurements to be compatible is 1 in 3.5 million. This gives no room for the possibility of a statistical fluctuation. This is known as the *Hubble constant tension H_0 problem* [3, 4]. There are two possible explanations for the tension. The first one is that there are unaccounted systematic errors in the analysis from SH0ES [5]. The other possibility relates to the breakdown of the standard ΛCDM model [6]. This would require the establishment of a new standard model of Cosmology that can solve the Hubble tension. However, this is not an easy task. Solving the Hubble constant tension is a necessary condition to be the new standard model, but it is by no means sufficient. The new standard model also needs to provide an accurate explanation of the phenomena that ΛCDM can describe. This includes, but is not limited to the existence of the CMB [7], the large-scale structure of the Universe [8], and the accelerated expansion of the Universe [9].

The possibility that the determination of H_0 is being affected by unaccounted systematic errors makes having a variety of observables crucial. Others do not share the systematic uncertainties of supernovas and cepheids. Thus, in this thesis, we will consider distance measurements from strong lensing and Baryon Acoustic Oscillations (BAO). We will start from [10]. The purpose of this paper was to carry out a consistency check of the distance-redshift relation determined by the supernova of the Pantheon catalogue [11] and the strong lensing measurements of the H0LiCOW collaboration [12]. The consistency check consists of starting from the Pantheon catalogue and predicting the H0LiCOW strong lensing distances. Then, it is possible to make comparisons and determine whether the results are consistent in a similar way in which we assess the compatibility of the H_0 determination between SH0ES 2022 and Planck 2018. The assumptions to predict the distances are that the Universe is spatially flat and to calibrate the absolute magnitude of the Pantheon supernova with the result from SH0ES 2022. This makes possible to evaluate if the analysis from the SH0ES collaboration is biased by unknown systematic errors. The premise for this is that since systematics on H0LiCOW and SH0ES act differently, then a comparison of their results would show if there are some unaccounted systematics. If the results are in agreement, it implies that there are no indications of unaccounted systematics. In [10], they showed that this is the case in both Pantheon and H0LiCOW. However, there is an unlikely scenario where the systematics can act in the same way, redshift, sign and magnitude. Thus, new analyses would make a more robust claim to these conclusions.

We will update the results from [10]. We will replace the Pantheon catalogue [11] with its new updated version, called Pantheon+ [13]. Furthermore, we will consider results from BAO observations. In particular, we will take the recent results from the DESI collaboration [14, 15]. While strong lensing observations give distances, BAO observations give distance ratios. In particular, they measure D_M/r_d and D_H/r_d where D_M is a distance called comoving transverse distance, $D_H = c/H(z)$ is the Hubble distance and $H(z)$ the Hubble factor which measures the expansion of the Universe at any point in history. Finally, r_d is the sound horizon. It is the distance that Baryon Acoustic Waves travelled from the Big Bang to the moment of recombination. Since baryons and photons are decoupled from recombination, this distance is fixed after the decoupling. These observables

give different results that are affected by different systematics from the ones from Supernovas.

The methodology to predict distances starting from the Pantheon+ catalogue relies upon the use of Gaussian Process (GP) interpolation. This builds a continuous version of the Pantheon+ catalogue. Thus, it builds a continuous version of the distance modulus that can be converted to luminosity distances and thus to other kinds of distances. This allows us to compare the observables of H0LiCOW and DESI with the predictions from Pantheon+. The predictions from Pantheon+ are model-independent and thus allow us to determine whether any dataset is being subject to unaccounted systematics. If Pantheon+ has unknown systematics, then its predictions for strong lensing distances and BAO distance ratios would not be compatible with H0LiCOW and DESI, respectively. However, there is still the possibility that two datasets are being subject to the same kind of systematics, at the same redshift, sign and magnitude [16]. Although this possibility is unlikely it cannot be discarded by comparing Pantheon+ with H0LiCOW. However, if we compare Pantheon+ with H0LiCOW and also with DESI BAO, and the level of agreement is good, it is an indication that there are no signs of unaccounted systematics in the three datasets. Therefore, it implies that the H_0 determination of the SH0ES collaboration is not affected by unaccounted systematics and thus, the origin of the Hubble constant tension is physical. The tests presented in this thesis and [10] are complementary of other systematic tests [17, 18, 19, 20] and to other papers assessing the sources of the systematics [21, 22, 23, 24, 25, 26, 27, 28]. Furthermore, the last result from the SH0ES collaboration [1], which is the one where we reached the critical point of having a 5σ C.L. tension, significantly reduced the systematics involved. Thus, as time goes on, it seems that the possibility of the tension having a physical nature becomes higher.

The thesis is divided in the following way: In Chapter 1, we give an introduction to background cosmology and the required tools to use Type 1a Supernova, Strong Lensing distances and Baryonic Acoustic Oscillations. In Chapter 2, we develop the theory of Type 1a Supernova and Baryonic Acoustic Oscillations. In Chapter 3, we briefly describe the strong lensing catalogues. Then, we describe the procedure to predict distances with Gaussian Processes starting from the Pantheon+ catalogue. Finally, we present the comparison between Strong Lensing data and Pantheon+. In Chapter 4, we describe the method to calibrate

the sound horizon r_d in a model-independent way. Then, we make the comparison between the Baryonic Acoustic Oscillation distance ratios and Pantheon+. Finally, in the conclusions, we present our final remarks.

Chapter 1

Background Cosmology

We start by giving an introduction to Background Cosmology and the required tools to use Supernova Type 1a, Strong Lensing and Baryon Acoustic Oscillations as cosmological probes.

1.1 The Cosmological Principle

The idea that a privileged observer does not exist is known as the Copernican principle. When we apply this principle to Cosmology, we naturally develop the concepts of isotropy and homogeneity. Isotropy means that the Universe has the same properties regardless of the direction in which we look. On the other hand, homogeneity means that the Universe has the same average density everywhere. However, when looking at the sky, we immediately can see that the Universe is neither isotropic nor homogeneous. There exist a large number of stars and galaxies with a vacuum around them. With this in mind, the Universe would not be able to hold the Copernican principle. Nevertheless, homogeneity and isotropy hold when looking at large scales (on the order of Megaparsecs) with just tiny variations of the order of 1 on 10^5. This is known as the cosmological principle, and as we can see, it is a corollary of the Copernican principle when applying it to Cosmology. This is a strong assumption since it also guarantees that the laws of Physics are Universal.

Starting from the cosmological principle, we can derive the Friedmann-Lemaitre-

Robertson-Walker (FLRW) metric [29]

$$ds^2 = -c^2dt^2 + a^2(t)\left(\frac{dr^2}{1-kr^2} + r^2(d\theta^2 + \sin^2\theta d\phi^2)\right), \tag{1.1}$$

where $a(t)$ is known as the scale factor and it depends on time. It has an important physical meaning. It quantifies how big the Universe is. At the moment of the Big Bang, it was $a(0) = 0$ and nowadays it is $(t_0) = a_0$, where the subindex zero refers to the current epoch. However, since a_0 is just a normalization factor, it is usual to set it to $a_0 = 1$.

Before moving on to the Friedmann equations, it is useful to introduce the concept of comoving coordinates. We were talking about the cosmological principle in the last paragraphs, where we stated that the Universe is isotropic and homogeneous. However, this is true in only one coordinate system, which is known as the comoving coordinate system. We can easily see this if we consider the Cosmic Microwave Background (CMB). This radiation satisfies the cosmological principle in the comoving system. However, if we move at a certain speed with respect to this coordinate system, we start detecting a dipole contribution of the CMB. This no longer respects the cosmological principle. Then, the only coordinate system where it is valid is the comoving system. In this system, the distance between two galaxies remains frozen in time. Thus, the comoving coordinates are the ones that expand in the same way as the Universe. Inside the FLRW metric (1.1), the comoving distance is given by r and it is the distance in this frame reference. If we want to derive the physical actual distance from this, we need to multiply the comoving distance with the scale factor $(D(t) = a(t)r)$.

1.2 The Friedmann equations

After selecting the FLRW metric, which is the one that fulfils the cosmological principle, we proceed to solve the Einstein equations

$$R_{\mu\nu} - \frac{1}{2}Rg_{\mu\nu} = 8\pi G T_{\mu\nu}, \tag{1.2}$$

where $R_{\mu\nu}$ is the Ricci tensor, R the Ricci scalar, and $T_{\mu\nu}$ the stress-energy tensor given by

$$T_{\mu\nu} = (\rho + p)u_\mu u_\nu + p g_{\mu\nu}, \tag{1.3}$$

where ρ is the density, p the pressure and u_μ the 4-velocity. Notice that we assumed the Universe comprises only perfect fluids. By starting from the FLRW metric (1.1) and computing the components of the Einstein equations, we derive the Friedmann equations

$$H^2 = \frac{8\pi G}{3}\rho - \frac{kc^2}{a^2}, \tag{1.4}$$

$$\dot{H} + H^2 = -\frac{4\pi G}{3}\left(\rho + \frac{3p}{c^2}\right), \tag{1.5}$$

where $H = \dot{a}/a$ is the Hubble factor. The first equation is known as the *first Friedmann equation* or just as the *Friedmann equation*. In contrast, the second one is known as the *second Friedmann equation*, the *Raychaudhuri equation* or the *acceleration equation*. We should note that the density and pressure in equations (1.4) and (1.5) refer to the total density and the total pressure.

We can derive an additional equation. Starting from the Bianchi identities [30]

$$\nabla_\alpha R^\beta{}_{\gamma\mu\nu} + \nabla_\mu R^\beta{}_{\gamma\nu\alpha} + \nabla_\nu R^\beta{}_{\gamma\alpha\mu} = 0, \tag{1.6}$$

where $R^\beta{}_{\gamma\mu\nu}$ is the Riemann curvature tensor tensor. By contracting β with μ, using the symmetries of the Riemann tensor and contracting γ and ν

$$\nabla_\alpha R - 2\nabla_\gamma R^\gamma{}_\alpha = 0, \tag{1.7}$$

which can be rewritten as

$$\nabla^\gamma\left(R_{\gamma\alpha} - \frac{1}{2}R g_{\gamma\alpha}\right) = 0, \tag{1.8}$$

then, the Einstein equations imply that

$$\nabla_\gamma T^{\gamma\alpha} = 0. \tag{1.9}$$

If the solve for the zeroth component of this equation, we get the density evolution equation

$$\dot{\rho} + 3H\rho(1+w) = 0, \tag{1.10}$$

with w the equation of state $w = p/(\rho c^2)$. If we assume that w is a constant

$$\rho(a) = \rho_0 a^{-3(1+w)}, \tag{1.11}$$

where the zeroth sub-index refers to the current time (we are setting $a_0 = 1$). It is important to mention that the set of equations (1.4), (1.5) and (1.10) are not independent. Only two of them are independent and the third one can be derived from the other two. We can see this by taking the derivative with respect to the time of equation (1.4). If we substitute $\dot{\rho}$ using equation (1.10), we get (1.5).

It is possible to rewrite the Friedmann equations with the density parameters. We need to define the critical density (ρ_c). It is given by the density the Universe has when its spatial curvature is equal to zero ($k = 0$). So,

$$\rho_c = \frac{3H^2}{8\pi G}, \tag{1.12}$$

and then the density parameters are defined by

$$\Omega = \rho/\rho_c = \frac{8\pi G\rho}{3H^2}, \tag{1.13}$$

and then the Friedmann equation (1.4) can be written as

$$\Omega + \Omega_k = 1, \tag{1.14}$$

where Ω_k is the curvature parameter

$$\Omega_k = -\frac{kc^2}{a^2H^2}. \tag{1.15}$$

1.2.1 Redshift

In this subsection, we will talk about the geodesics in the FLRW metric. We will also introduce an important concept called redshift which will be critical in the remainder of the thesis. We define $p^\mu = dx^\mu/d\lambda$ as the 4-momentum where λ is a parameter. Then, the geodesic equation is [30]

$$\frac{dp^\mu}{d\lambda} + \Gamma^\mu{}_{\alpha\beta}p^\alpha p^\beta = 0, \tag{1.16}$$

and also

$$p \cdot p = g_{\mu\nu}p^\mu p^\nu = -\frac{E^2}{c^2} + p^2 = -m^2c^2. \tag{1.17}$$

We will focus on the case of photons. Their mass is zero. The zeroth compo-

nent of the geodesic equation is

$$\frac{dp^0}{d\lambda} + \frac{a\dot{a}}{c}\delta_{ij}p^i p^j = 0, \tag{1.18}$$

where the Latin indexes i, j run over the spatial components. Then, since photons are massless $p^0 = E/c = p$

$$\frac{dp}{d\lambda} + \frac{H}{c}g_{ij}p^i p^j = 0, \tag{1.19}$$

where we can write $\frac{dp}{d\lambda} = \frac{dp}{dx^0}\frac{dx^0}{d\lambda} = \frac{dp}{dt}E$

$$\frac{dp}{dt} + Hp = 0, \tag{1.20}$$

which has a solution

$$p = \frac{C}{a}, \tag{1.21}$$

with C a constant. For a photon, $E = \frac{hc}{\lambda}$ with h the Planck constant and λ the wavelength. Thus

$$\frac{a_{\text{emitted}}}{a_{\text{observed}}} = \frac{\lambda_{\text{emitted}}}{\lambda_{\text{observed}}} := \frac{1}{1+z}, \tag{1.22}$$

where z is known as redshift. Since we set the current scale factor to 1, we can write

$$a = \frac{1}{1+z}, \tag{1.23}$$

and then we can write the scale factor in terms of a quantity that can be measured, the redshift.

1.3 Cosmological Parameters

In this section, we will study how the first Friedmann equation (1.4) can be written in terms of a set of parameters.

1.3.1 Density parameters

We will focus on the density parameters evaluated at present. Moreover, we will consider a set of different species that can range from radiation to matter. We will denote each species with a different index i. Then, the density parameter at

the present for a given species is

$$\Omega_{i0} = \frac{8\pi G \rho_i a^{3(1+w_i)}}{3H_0^2}, \tag{1.24}$$

where w_i is the equation of state of the species and H_0 is the Hubble factor evaluated at constant time. If we divide the first Friedmann equation (1.4) with H_0^2

$$\left(\frac{H}{H_0}\right)^2 = \sum_i \Omega_{0i} a^{-3(1+w_i)} + \Omega_{0k}, \tag{1.25}$$

and the sum goes over all the species considered. We are considering that each species does not interact with the other ones. This enables us to write the density evolution equation (1.10) for each species as

$$\dot{\rho}_i + 3H\rho_i(1 + w_i) = 0. \tag{1.26}$$

By evaluating equation (1.25) at the present, we get the closure equation

$$\sum_i \Omega_{0i} + \Omega_{0k} = 1, \tag{1.27}$$

which indicates that not all the density parameters are independent. One of them can be written in terms of the other ones. This reduces the parameter space by one. In the remainder of this thesis, we will omit the zeroth index when talking about density parameters since we will refer to them at present.

1.3.2 The Hubble constant

The remaining cosmological parameter relevant to background Cosmology is known as the Hubble constant ($H(a = 1) = H_0$). It is defined as the Hubble parameter evaluated at present. Thus, it measures the current rate of expansion of the Universe. It is one of the most important parameters in Cosmology and its measurement has opened the door for a new problem in Cosmology. This is called *the Hubble constant problem*. We will talk more about this problem in the following sections and chapters. However, in this sub-section, we will outline the problem. This problem, which has become a crisis in Cosmology started by measuring the Hubble constant with two different methods. We have methods that do not assume a specific model of Cosmology. These give a model-independent measurement of the Hubble constant but can be subject to unknown systematic

effects. The most important result from this method is the one given by the SH0ES collaboration. By using Type 1a Supernova (SNeIa) and cepheid stars, they measured a value of [1]

$$H_0 = 73.04 \pm 1.04 \,\text{km/s/Mpc}. \tag{1.28}$$

The SH0ES collaboration has made continuous efforts to take into account all the possible systematic errors and this result is the best current model-independent measurement of H_0. On the other hand, we can consider model-dependent methods. The most accurate measurement of H_0 with this method is given with the Cosmic Microwave Background (CMB) Planck dataset. This is [2]

$$H_0 = 67.4 \pm 0.4 \,\text{km/s/Mpc}, \tag{1.29}$$

which gives a sub-percent determination of H_0. The Hubble constant problem arises when we consider the posterior probabilities of H_0 in both results to see whether they are consistent with each other. It turned out that both determinations are in a 5σ C.L. tension [1].

The tension between model-dependent and model-independent methods has been growing in the last decade with increasing precision in the measurements. However, reaching a value of 5σ becomes a critical issue for Cosmology. The interpretation of a 5σ C.L. tension is that both measurements have a 1 in 3.5 million probability of compatibility. This can have two possible explanations

1. The SH0ES collaboration measurement of H_0 is being severely affected by unknown systematic errors.

2. The assumed cosmological model by Planck is incomplete and we need to change the standard model of Cosmology.

The first possibility starts to get less likely with time since the SH0ES collaboration along with others is working to reduce as much as possible the systematic errors and by doing so the Hubble tension remains there. This gives the possibility of needing a new standard model of Cosmology. We will talk about this model in the next section which is called the ΛCDM *model*.

1.4 The Standard Model ΛCDM

ΛCDM is the name of the standard model of Cosmology. It is the one with the highest amount of observational evidence. Thus, it is important to study and comprehend this model. The basic idea of the ΛCDM model is that most of the Universe energy content comes from dark energy in the form of a cosmological constant Λ and *cold dark matter (CDM)*. Dark energy is a hypothetical perfect fluid with a negative equation of state equal to minus 1 ($\omega_\Lambda = -1$). This implies that the pressure is negative. This fact causes the observed accelerated expansion of the Universe. The second dominant component is cold dark matter. The term dark matter means that it does not interact with the electromagnetic interaction. Conversely, cold means that it is non-relativistic. Then, this matter moves much slower than the speed of light and thus, it has the same equation of state as Baryonic matter. Apart from this, the Universe is composed of Baryonic matter and radiation (neutrinos, photons and other relativistic particles). The equation of state of the 4 species is

1. Dark energy cosmological constant (Λ): $w = -1$
2. Cold dark matter (CDM): $w = 0$
3. Baryonic matter (b): $w = 0$
4. Radiation (r): $w = 1/3$

Since CDM and baryonic matter have the same w, they have the same background evolution. Assuming that the Universe is composed of these 4 components, the Friedmann equation in terms of Cosmological parameters (1.25) is

$$H(z) = H_0\sqrt{\Omega_b(1+z)^3 + \Omega_{cdm}(1+z)^3 + \Omega_r(1+z)^4 + \Omega_k(1+z)^2 + \Omega_\Lambda}, \quad (1.30)$$

and since the evolution of baryonic and cold dark matter is the same, we can define $\Omega_m = \Omega_b + \Omega_{cdm}$ as a new matter cosmological parameter. Then

$$H(z) = H_0\sqrt{\Omega_m(1+z)^3 + \Omega_r(1+z)^4 + \Omega_k(1+z)^2 + \Omega_\Lambda}, \quad (1.31)$$

and for the closure relation

$$\Omega_m + \Omega_r + \Omega_k + \Omega_\Lambda = 1, \quad (1.32)$$

which implies that the ΛCDM model has a total of four parameters. However, in the present thesis, we will work at low redshift. And since $\Omega_r \sim 10^{-5}$ [2, 31], we can approximate $\Omega_r \approx 0$. Thus, we will neglect the contributions of radiation since we will work at low redshift. In addition to this, we will set $\Omega_k = 0$. There is observational evidence that $\Omega_k \approx 0$ [2, 31, 32]. Also, inflation drives Ω_k close to the zero value. These facts enable us to also set $\Omega_k = 0$. Then, we can write the Hubble factor of the ΛCDM model in terms of only two background parameters

$$H(z) = H_0\sqrt{\Omega_m(1+z)^3 + (1-\Omega_m)}, \tag{1.33}$$

where we used the closure relation. The parameter vector of ΛCDM is then $\Theta = \{H_0, \Omega_m\}$.

1.5 Distances in Cosmology

There are several ways to measure distance in Cosmology. We will introduce some of the most important ones in this section.

1.5.1 Comoving Distance

As we mentioned, it is a distance that does not grow with time. Let us consider a comoving distance D_C to a light source. By definition, $D_f = aD_C$ is the physical distance. In a time differential dt, light moves a differential physical distance dD_f. Then, in this interval, it moves a differential moving distance

$$dD_C = \frac{dD_f}{a} = \frac{cdt}{a}, \tag{1.34}$$

where we used the fact that light travels at the speed of light. By integrating, we derive the comoving distance

$$D_C(t) = c\int_t^{t_0} \frac{dt'}{a(t')}, \tag{1.35}$$

where we are integrating from the emission time to the present. By performing the variable change from time to redshift

$$D_C(z) = c\int_0^z \frac{dz}{H(z)}, \tag{1.36}$$

where $H(z)$ is the Hubble factor. Then, by knowing the expression for $H(z)$, we can compute the comoving distance. For example, we can use the Hubble factor of the ΛCDM model (1.33).

1.5.2 Transverse Comoving Distance

To define this distance, we need to consider two events at the same redshift but separated by an angle $\delta\phi$. The comoving distance between these two events is given by $D_M\delta\phi$, where D_M is the transverse comoving distance. It is related to the comoving distance by [33]

$$D_M(z) = \begin{cases} \dfrac{D_H}{\sqrt{\Omega_k}} \sinh\left(\sqrt{\Omega_k}\dfrac{D_C}{D_H}\right) & \text{if} \quad \Omega_k > 0, \\ D_C & \text{if} \quad \Omega_k = 0, \\ \dfrac{D_H}{\sqrt{|\Omega_k|}} \sin\left(\sqrt{|\Omega_k|}\dfrac{D_C}{D_H}\right) & \text{if} \quad \Omega_k < 0, \end{cases} \tag{1.37}$$

where $D_H = c/H_0$ is known as the Hubble distance. This distance is important because the remaining ones that we are introducing in this section are given in terms of this one.

1.5.3 Angular Diameter Distance

This distance is the ratio of an object's transverse physical size to its angular size in radians. It is useful to turn angular separations into proper separations. Its expression is given by [33]

$$D_A(z) = \frac{D_M(z)}{1+z}, \tag{1.38}$$

and as we can see, it does not increase indefinitely with redshift. The formula implies that the most distant objects have a bigger angular size. It can be measured by computing

$$D_A(z) = \frac{x}{\delta\phi}, \tag{1.39}$$

where x is the physical transverse size and $\delta\phi$ is the angular size.

1.5.4 Luminosity Distance

This distance is computed by measuring the flux and the luminosity of an object integrated over all frequencies

$$D_L = \sqrt{\frac{L}{4\pi F}}, \tag{1.40}$$

where L is the luminosity and F the flux. Furthermore, it is given in terms of the transverse comoving distance with [33]

$$D_L(z) = (1+z)D_M(z) = (1+z)^2 D_A(z). \tag{1.41}$$

Also, the apparent magnitude m of an electromagnetic radiation source is defined as the base 10 logarithm of the ratio between the apparent flux and the one of the bright star Vega. On the other hand, the absolute magnitude M is the relative magnitude given at 10 parsecs (pc) from the source. The distance modulus μ is given by the difference between the relative and absolute magnitudes [33]

$$\mu(z) = m(z) - M = 5\log_{10}\left(\frac{D_L(z)}{10\text{ pc}}\right). \tag{1.42}$$

1.6 The Hubble Constant Tension Problem

We provided a brief introduction to the Hubble constant tension in subsection 1.3.2. In this section, we will expand the explanation of this problem. This problem has arisen recently in Cosmology with the increasing precision to measure the cosmological parameters. A precise constrain in the Hubble constant H_0 is important since it is the inverse of the age of the Universe. Thus, an accurate measurement of it can lead to an accurate measurement of the age of the Universe. We will start this section by providing a brief overview of how the model-independent and model-independent methods to determine H_0 work. The model-independent method relies upon the cosmic distance ladder while the model-dependent one relies on constraints in the anisotropies of the CMB.

1.6.1 The Cosmic Distance Ladder

The Hubble constant can be measured with the cosmic distance ladder with the use of three rungs. These rungs are the following [1]

1. Geometric distance measurements to standardized Cepheid variables.
2. Standardized Cepheids and colocated SNe Ia in nearby galaxies.
3. SNe Ia in the Hubble flow.

The basic idea is to use standard candles. This kind of object has the same intrinsic Luminosity. Thus, by measuring the Luminosity ratios of two standard candles, we can determine the distance ratio with the squared law distance relation. By starting from the equation (1.40), if we consider the ratio of the distances of two standard candles with a known Luminosity L

$$\frac{D_{L1}}{D_{L2}} = \sqrt{\frac{F_2}{F_1}}, \tag{1.43}$$

and then by measuring the ratio of flux, we can determine the ratio of their distances. Equivalently, we can measure the relative magnitude of two standard candles. Since they have the same intrinsic luminosity, they have the same absolute magnitude M

$$m_1 - m_2 = 5 \log_{10} \left(\frac{D_{L1}}{D_{L2}} \right), \tag{1.44}$$

and then the distance ratio is given by

$$\frac{D_{L1}}{D_{L2}} = 10^{\frac{m_1 - m_2}{5}}. \tag{1.45}$$

Then, with the standard candle method, we can determine the distance to all of them if we can at least measure the distance to one of the candles. This is not an easy task since it requires the determination of the distance by other methods like the parallax method or the measurement of the absolute magnitude. Two types of standard candles are frequently used in Cosmology: cepheid variable stars and supernova type 1a (SNeIa).

Cepheid variable stars are pulsating variable stars that brighten and dim at periodic intervals. For a set of $\mathbf{P}$ periods and mean relative magnitudes $\mathbf{m_i}$, the pulsation equation P-L is of the form [34]

$$\mathbf{m_i} = zp_{X,i} + b_X \log \mathbf{P}, \tag{1.46}$$

where $zp_{X,i}$ is the intercept of the P-L relation and b_X the slope of the passband X. Thus, we can derive the relative magnitude given the pulsation periods by

fitting the data. On the other hand, SNeIa are extremely luminous explosions. They form when a white dwarf is accreting material from a companion star. It explodes when it reaches the Chandrasekhar limit, causing an extremely bright explosion that can be observed. The fact that the explosion is predictable makes it a standard candle. They follow a particular light curve showing an increase in the brightness until achieving the maximum. Then, the brightness exhibits a continuous decrease with time. An example of this behaviour can be seen in Figure 1.4 from [35]. The relative magnitude of the SNeIa is then determined from the maximum of the light curve.

The first rung consists of calibrating Cepheid variables from Geometric distance measurements. This enables the determination of the distance to these events and calibrates its absolute magnitude [36, 37]. For example, this method was applied for the Cepheids hosted in the spiral galaxy NGC 4258 [38, 39]. The second rung uses standardized cepheids to calibrate the absolute luminosity of SNeIa. If we consider a host of both a cepheid and a SNeIa, the relative magnitude of the SNeIa is [1]

$$m^0_{B,i} = \mu_{0,i} + M^0_B, \tag{1.47}$$

where $m^0_{B_i}$ is the maximum apparent magnitude of the SNeIa, M^0_B the absolute magnitude for SNeIa and $\mu_{0,i}$ the distance modulus of the standardized cepheid. This equation enables us to determine the absolute magnitude for SNeIa (M^0_B) and to use this result for the SNeIa in the third rung. Finally, the third rung works with SNeIa in the Hubble flow. For this rung. the following expression is useful [1]

$$\alpha_B = \log cz \left(1 + \frac{1}{2}(1-q_0)z - \frac{1}{6}(1-q_0-3q_0^2+j_0)z^2 + O(z^3)\right) - 0.2m^0_B, \tag{1.48}$$

where c is the speed of light, $q_0 = -\dfrac{\ddot{a}_0 a_0}{\dot{a}_0^2}$ is the deceleration parameter and $j_0 = \dfrac{\dddot{a}_0 a_0^2}{\dot{a}_0^3}$ the jerk parameter. This expression comes from expanding the luminosity distance in Taylor's series. Finally, the determination of the Hubble constant is given by [1]

$$\log H_0 = 0.2M^0_B + \alpha_B + 5. \tag{1.49}$$

Notice that in this method, we never need to assume a specific Cosmological

model. Thus, the determination of H_0 is a model-independent one.

1.6.2 CMB anisotropies

The method to constrain H_0 using the CMB consists of three steps [6]

1. Determining the Baryon and radiation density to allow the calculation of the sound horizon $r_d^\star$ at the redshift of the CMB last-scattering.

2. Determining the angular size on the last-scattering surface $\theta_d^\star$ from the spacing between the acoustic CMB peaks and determining the comoving angular diameter distance at last scattering $D_A^\star = r_d^\star/\theta_d^\star$

3. Adjust the remaining density-free parameter in the model to derive the distance
$$D_A^\star = \int_0^{z_\star} \frac{dz}{H(z)}. \tag{1.50}$$
This last step enables a determination of $H(z)$ for all redshifts. So, it also gives the Hubble constant $H_0 = H(z = 0)$.

The sound horizon at the surface of the last scattering is given by

$$r_d^\star = \int_0^{t_\star} dt \frac{c_s(t)}{a(t)} = \int_{z_\star}^{\infty} dz \frac{c_s(z)}{H(z)}, \tag{1.51}$$

where c_s is the sound speed and $z_\star$ and $t_\star$ are the redshift and time of the last scattering surface. They are the corresponding values when the optical depth of Thompson scattering is equal to one. The sound horizon is given by

$$c_s(z) = \frac{\partial P}{\partial \rho} = \frac{c^2}{3}\left(1 + \frac{\partial \rho_b}{\partial \rho_\gamma}\right)^{-1}, \tag{1.52}$$

and then it depends on the ratio of Baryon to photon density. Notice that we only included Baryons and photons. We did not consider dark matter or neutrinos. This is because the Thompson scattering is an electromagnetic interaction and both dark matter and neutrinos do not interact electromagnetically. The radiation density can be determined from the temperature of the CMB [40, 41]. Thus, we only need to determine the Baryon content to derive the sound horizon.

Apart from computing the sound horizon, we also need to derive the Hubble factor $H(z)$. In principle, we can perform a Taylor series expansion of $H(z)$ as

we did in equation (1.48). However, we would need to expand around the redshift of the last scattering $z_\star$ instead of the current redshift $z = 0$. This would allow us to constrain $H(z_\star)$ but not the Hubble constant H_0. The other option is to expand around $z = 0$ but this would be impractical since we would need to write a huge (or even infinite) amount of higher-order terms dependent on z to have a good expansion of $H(z)$ that works from the last scattering surface to the Big Bang. Then, the only practical option to constrain H_0 is to assume a specific Cosmological model and thus an expression for $H(z)$. If we consider the standard ΛCDM model, we take (1.30). Thus, as we can see, this method will be model-dependent in contrast to the cosmic distance ladder one.

The determination of the mean density of neutrinos can be written as a function of the photon temperature. The other ones that we need to determine are the mean density of matter and the Cosmological constant. However, the Cosmological constant does not affect the sound horizon [6]. It is customary to write the following quantities

$$\omega_m = \Omega_m h^2, \tag{1.53}$$

$$\omega_b = \Omega_b h^2, \tag{1.54}$$

$$\omega_{cdm} = \Omega_{cdm} h^2, \tag{1.55}$$

where $h = H_0/(100\text{km/s/Mpc})$ is the adimensional Hubble constant.

We can determine the cosmological parameters from the CMB power spectrum. By changing the value of ω_m, H_0 or the other parameters, the form of the power spectrum also changes. Thus, by measuring the power spectrum, we can directly constrain the parameters. We briefly describe how ω_m, ω_b and H_0 can affect the power spectrum.

The primary effect of ω_m on the power spectrum comes from the Integrated Sachs-Wolfe (ISW) effect and the gravitational lensing smoothing of the spectrum [42]. When Fourier modes cross the horizon, the gravitational potential decay gives a driver of the oscillation close to resonance. The bigger the matter-to-photon ratio at the horizon crossing, the smaller the oscillation amplitude.

On the other hand, an increasing Baryon-to-photon ratio reduces the pressure-to-density ratio. This changes the zero point of the acoustic oscillations [6, 42]. Modes compressing into the potential walls at decoupling compress even more [6] and the ones rarifying do not do it much. This boosts the compression peaks and suppresses the rarefaction ones in the CMB temperature power spectrum. Furthermore, changing ω_b also changes the density of free electrons at recombination. As we can see, the effects of ω_m and ω_b are not the same in the CMB power spectrum. This contrasts the background evolution where Baryonic and total matter had the same background evolution.

The characteristic angular size of the fluctuations in the CMB $\theta^\star = r^\star/D_A^\star$ are well determined at better than 0.1% precision [43]. The sound horizon is determined by the redshift of recombination $z_\star$, ω_m and ω_b. Then, the constraint on $\theta^\star$ comes from a constraint to the distance of the surface of the last scattering. This gives a determination of a 3-dimensional subspace $\omega_m - \omega_b - h$ [42]. After marginalizing over ω_b, a strong degeneracy between ω_m and h appears and can be approximated as $\Omega_m h^3 = \text{constant}$ [42].

The characteristic angular size of the fluctuations in the CMB can be derived from the spacing of the peak spacing [6, 44]. This is given by [6]

$$\theta_s^\star = \frac{\pi}{\Delta\ell}, \tag{1.56}$$

where $\ell = kD_A^\star$ and k are the Fourier modes. Then, $\Delta\ell$ refers to the peak spacing.

Therefore, after computing $r_d^\star$ and determining $\theta_d^\star$ from the peak spacing, we can derive the angular diameter distance to the last scattering surface

$$D_A^\star(z_\star) = \int_0^{z_\star} \frac{dz}{H(z)}, \tag{1.57}$$

and after specifying the cosmological parameters, $H(z)$ is specified for all redshift and thus, it is also specified for $z = 0$ which implies a constraint in the Hubble constant H_0.

1.6.3 The Evolution of the Hubble Constant Tension with Time

As we were describing, both methods allow us to determine the value of the Hubble constant. However, the cosmic distance ladder provides a model-independent constraint while CMB anisotropies provide a ΛCDM constraint.

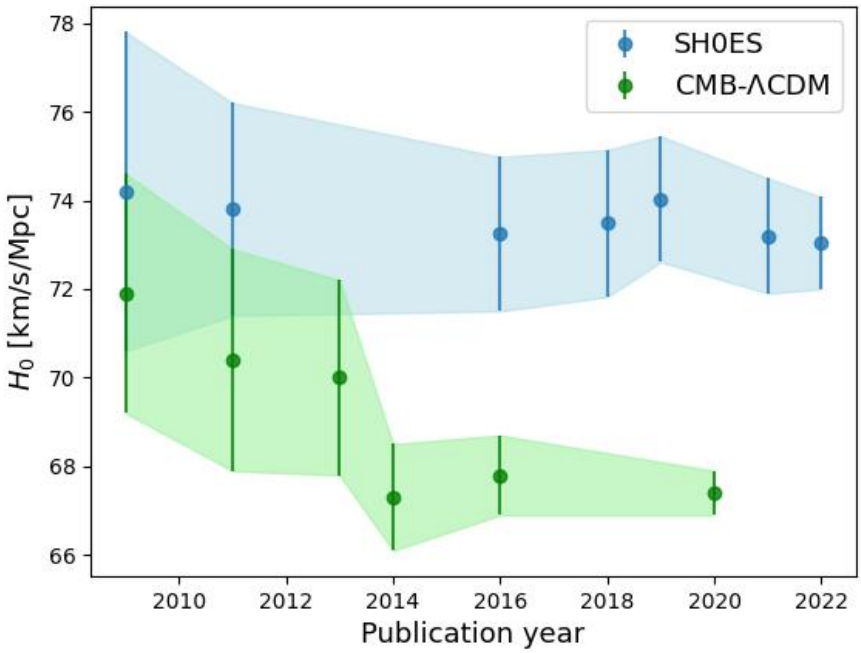

Figure 1.1: Mean values of the Hubble constant along with the 1σ C.L. uncertainties as a function of publication year. We included the results from the SH0ES collaboration using the cosmic distance ladder and from WMAP and Planck using the CMB anisotropies and the standard model ΛCDM. For SH0ES, we included the results from [34, 45, 46, 47, 48, 36, 1] while for WMAP and Planck we considered [49, 50, 51, 43, 52, 2].

We present the mean values and the 1σ C.L. uncertainties for the SH0ES collaboration that uses the cosmic distance ladder method and for the WMAP and Planck collaborations that use the CMB anisotropies method. As we can see, in 2009 and 2011, the results from both methods agree at 1σ C.L. However, since then, the difference between both has been growing. It grew until it reached a critical point in 2022 with the results from [1] where the difference between the cosmic distance ladder and CMB anisotropies reached a difference of 0.176 ± 0.035 in units of $\Delta 5 \log H_0$ which implies a difference of 5.0σ [1]. This

is interpreted as a 1 in 3.5 million probability that both results are consistent. Thus, this hints at considering new alternatives to the standard ΛCDM model. Furthermore, a recent result, which is currently under review provides an update on the last SH0ES determination on H_0 [1]. By using the small magellanic cloud cepheids observed with the Hubble spatial telescope as a new anchor for the cosmic distance ladder, they derived a result of $H_0 = 73.17 \pm 0.86\,\mathrm{km/s/Mpc}$ [53]. This gives a tension of 5.8σ with respect to the ΛCDM Planck 2018 result [2]. Thus, this gives more evidence to the possibility of physics beyond the ΛCDM model.

As we can see, the Hubble constant tension problem is a critical issue that challenges the standard ΛCDM model. It provides strong evidence for the need for a new standard model of Cosmology. However, it is still the possibility that the cosmic distance ladder results are being severely biased by unknown systematic errors [5]. This possibility is becoming less likely with time since the SH0ES collaboration has been working on taking into account and reducing as much as possible the systematic errors [1]. In this thesis, we will focus on a consistency test on the distance-redshift relation measured by Pantheon+ [13], SNeIa compilations and a Baryon Acoustic Oscillations (BAO) compilation: BAO DESI 2024 [14, 15]. This expands the previous consistency tests performed [10] with the distance-redshift relation measured by Pantheon [11] and time delay and lens distance measurements from H0LiCOW [12, 54].

1.7 Bayesian Analysis in Cosmology

In this section, we will briefly summarize how to constrain the cosmological parameters of a model given some data. We start with the Bayes theorem

$$P(\mathbf{\Theta}|\mathbf{d}, \mathcal{M}) = \frac{P(\mathbf{\Theta}|\mathcal{M})P(\mathbf{d}|\mathbf{\Theta}, \mathcal{M})}{P(\mathbf{d}|\mathcal{M})}, \tag{1.58}$$

where $\mathbf{\Theta}$ represents the vector of Cosmological parameters, $\mathbf{d}$ the data vector and $\mathcal{M}$ is a specific cosmological model. $P(\mathbf{d}|\mathbf{\Theta}, \mathcal{M})$ is the likelihood probability and it quantifies the probability of the data being correct assuming a given value of the parameter vector and that the model $\mathcal{M}$ is correct. $P(\mathbf{\Theta}|\mathcal{M})$ is the prior probability and represents the values that a given parameter can physically take. To avoid introducing biases to the results, it is usual to take uniform probabili-

ties for the parameters. For example, for the Hubble constant H_0, we can take $H_0 \sim \mathcal{U}(0, 100)$ km/s/Mpc. This will let the data choose the correct value of H_0. We can also reduce the interval as long as we keep considering the tails of the parameter probability distribution function (pdf). $P(\mathbf{d}|\mathcal{M})$ is the evidence and it does not depend on the vector parameter $\mathbf{\Theta}$. It is a normalization constant that can be ignored if we are only interested in constraining the Cosmological parameters. However, this constant is important for model selection since the model with the highest evidence is also the preferred one by the data. For example, if we want to compare the standard ΛCDM model with an alternative one, we need to compute the evidence for both and the preferred one will be the one having the highest evidence. Finally, $P(\mathbf{\Theta}|\mathbf{d}, \mathcal{M})$ is the posterior probability. It quantifies the probability of the parameter vector given the cosmological model and the data. This is the quantity in which we are interested when constraining cosmological parameters. If we assume that the data is Gaussian, which is a reasonable assumption due to the central limit theorem, we have, for a single event [55]

$$P(\{y, z\}|\mathbf{\Theta}, \mathcal{M}) = \frac{1}{\sqrt{2\pi\sigma^2_{\text{observational}}(z)}} \exp\left(-\frac{(y_{\text{observational}}(z) - y_{\text{theoretical}}(z, \mathbf{\Theta}))^2}{2\sigma^2_{\text{observational}}(z)}\right), \tag{1.59}$$

where $y_{\text{observational}}(z)$ is the mean observational value of a cosmological observable. This can be the relative magnitude, a distance ratio or any quantity that can be measured. $y_{\text{theoretical}}(z, \mathbf{\Theta})$ is the value of the same quantity but computed from the model $\mathcal{M}$. It depends on both the redshift and the parameter vector $\mathbf{\Theta}$. Finally, $\sigma_{\text{observational}}$ is the standard deviation of the cosmological observable. We can simplify the Bayes theorem if we apply the natural logarithm to both sides. Moreover, let us consider N events and that they are independent of each other. After this, we can write

$$\ln P(\mathbf{y}, \mathbf{z}|\mathbf{\Theta}, \mathcal{M}) = \sum_{n=1}^{N}\left(\frac{1}{\sqrt{2\pi\sigma_n^2(z)}}\right) - \frac{1}{2}\sum_{n=1}^{N}\left(\frac{y_{\text{observational, n}}(z) - y_n(z, \mathbf{\Theta})}{\sigma^2_{\text{observational, n}}(z)}\right)^2, \tag{1.60}$$

the sum in the second term is known as the χ^2. This expression is valid if the measurements are not correlated with each other. In general, we have

$$\ln P(\mathbf{\Theta}|\mathbf{d}, \mathcal{M}) \propto -\frac{1}{2}\Delta\mathbf{y}^T \cdot C^{-1} \cdot \Delta\mathbf{y}, \tag{1.61}$$

where we have dropped the terms that would give a constant. Also $\Delta\mathbf{y}$ is given by

$$\Delta\mathbf{y} = \mathbf{y}_{\text{observational}} - \mathbf{y}_{\text{theoretical}}, \tag{1.62}$$

is the difference between the observational and theoretical values of the cosmological observable. Also, C is the covariance matrix that includes the variances in the diagonal. The off-diagonal terms include the possible covariances between all the pairs of values. We can define the χ^2 function as

$$\chi^2 = \frac{1}{2}\Delta\mathbf{y}^T \cdot C^{-1} \cdot \Delta\mathbf{y}. \tag{1.63}$$

The best-fit value of the parameter vector corresponds to the maximum of the posterior probability. Then, equation (**??**) implies that the best-fit value also corresponds to the minimum of the χ^2 function. To determine the mean value and the standard deviation, assuming that the parameters are Gaussian, it is common to use Monte Carlo Markov Chain Methods (MCMC).

In principle, we can explore the parameter space by taking hypercubes and evaluating the posterior in the centre of each cube. If the number of hypercubes is sufficiently big, we will successfully determine the mean value and uncertainty. However, there are more efficient methods. One famous method is Metropolis-Hastings [56]. The idea is to start at a random point in the parameter space, and then move randomly to a nearby point. If the posterior probability of the new point is bigger than the previous one, we keep it. Otherwise, we keep it with probability $P(X(t+1))/P(X(t))$ where $P(X(t))$ is the posterior probability in the initial point and $P(X(t+1))$ is the probability in the subsequent point. Thus, this method tends to favour points with increasing posterior probability. This helps to explore high-probability regions efficiently. Monte Carlo comes from the random nature and Markov chain comes from the fact that the chain of points that we are creating depends on the immediate previous point. Since we are exploring the parameter space at random, we can call this exploration a random walker. By taking several to a lot of random walkers and letting them explore the parameter space for enough time, we would approximate the posterior probability distribution function. This will then enable us to determine the mean values along with the uncertainties and correlation of the parameters.

Chapter 2

Type 1a Supernova (SNeIa) and Baryon Acoustic Oscillations (BAO)

In this chapter, we will discuss how SNeIa and BAO can be used as Cosmological tools to constrain the Cosmological parameters and how to determine the distances to these objects.

2.1 Type 1a Supernova (SNeIa)

Supernova are objects that explode under the same conditions. Their luminosity starts to increase until they get to a maximum. This increase occurs in a matter of weeks and it is followed by a decrease in luminosity that lasts for months. In the 1940s, it was discovered that there were at least two kinds of supernovas. Those with hydrogen features were denominated Type II whereas those without were denominated Type I [57]. With an improved quality of the observations, Type I supernovas were further divided into type Ia, Ib, and Ic. SNeIa is a supernova with a strong absorption feature and SNeIb and SNeIc do not have it [58]. Furthermore, SNeIa comes from thermonuclear explosions of low-mass stars [58].

In figure 2.1, we can see an example of the light curve for an SNeIa event. Although the explosion of SNeIa events occurs at the same point (when the white dwarf reaches the Chandrasekhar limit), the intrinsic determined absolute magnitude is not the same for different events [59]. They have to go over a process of standardisation. When measuring SNeIa, three pass-bands are used: the blue

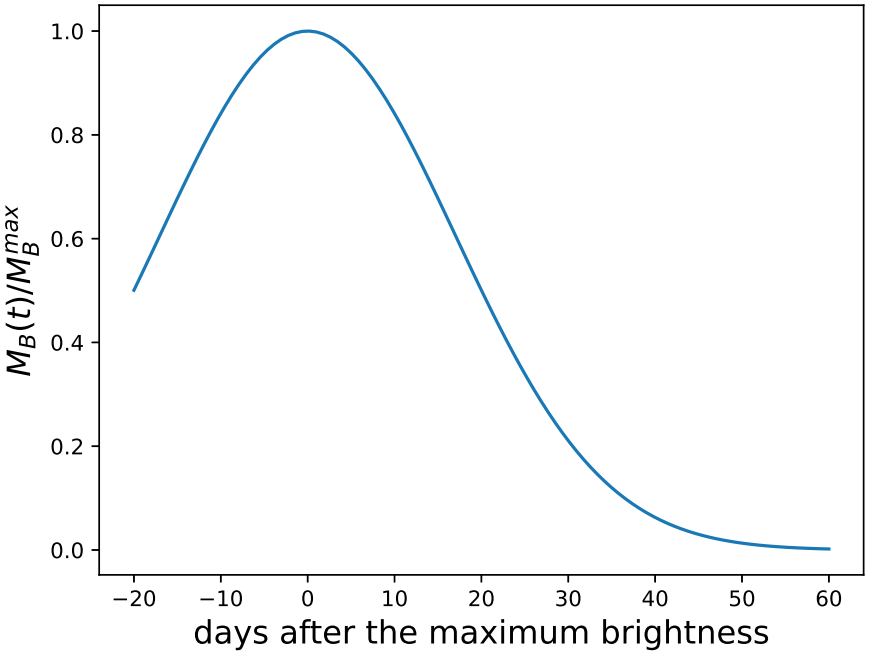

Figure 2.1: Example of a light curve for a SNeIa

passband (B), the visual passband (V) and the infrared passband (I). For SNeIa to work as standard candles, the absolute magnitude should be equal to every one of them. However, when computing the intrinsic absolute magnitude for each passband and different SNeIa, it was found that they were not the same [59].

However, the absolute magnitude can be corrected if we take into consideration the decline rate parameter $\Delta m_{15}(B)$ which is defined as the decay of the relative magnitude 15 days after the maximum in comparison to the maximum for the B passband. It was discovered that a dimmer SNeIa falls more rapidly than brighter ones [60]. By considering this, the dispersion of the absolute magnitude is reduced [61]. After performing correction in the peak brightness, it is possible to use SNeIa as standard candles [9].

We will see now how the Hubble constant H_0 and the absolute magnitude M are degenerate with SNeIa. Let us define $E(z) = H(z)/H_0$, the adimensional Hubble factor. If we substitute this in expression (1.42)

$$m(z) = M + 5\log_{10}\left((1+z)\int_0^z \frac{dz'}{E(z')}\right) + 5\log_{10}\left(\frac{c}{H_0(10\,\mathrm{pc})}\right), \tag{2.1}$$

where we are assuming that the Universe is spatially flat. SNeIa catalogues provide a measurement of the relative magnitude m. Thus, to study a theoretical model or even when performing model-independent studies, we get a degeneracy between M and H_0, we can define

$$\mathcal{M} = M + 5\log_{10}\left(\frac{c}{H_0(10\,\mathrm{pc})}\right), \tag{2.2}$$

and then

$$m(z) = \mathcal{M} + 5\log_{10}\left((1+z)\int_0^z \frac{dz'}{E(z')}\right), \tag{2.3}$$

and then from SNeIa data only, we can just constrain $\mathcal{M}$ and the parameters contained in $E(z)$. For a given value of $\mathcal{M}$, we will have a set of values of M and H_0. This is the source of the degeneracy. To break it, we need to determine the absolute magnitude and then, we can constrain the Hubble constant. As we were saying, it is possible to calibrate the value of M with cepheids. We need to find SNeIa events in the same galaxies as Cepheid variables. These Cepheids were previously calibrated using geometric methods after finding some of them close enough to the Earth. This enables us to determine the distances to them by calibrating the absolute magnitude of cepheids using geometric tools. Finally, using the calibrated cepheid variables, we go up in the rung of the cosmic distance ladder and we calibrate the absolute magnitude for SNeIa M. Thus, we can get the values of the distance modulus $\mu(z)$ and we can finally constrain the cosmological parameters

$$\mu(z) = m(z) - M = 5\log_{10}\left(\frac{(1+z)c}{H_0(10\,\mathrm{pc})}\int_0^z \frac{dz'}{E(z')}\right), \tag{2.4}$$

where we can finally use the SNeIa events as standard candles considering that the relative magnitudes are the corrected ones. We close this section by introducing the catalogue that we will use for this thesis (Pantheon+) and its predecessor (Pantheon).

2.1.1 The Pantheon Catalogue

The Pantheon catalogue is a compilation of 1048 SNeIa in the redshift range $0.01 < z < 2.3$ [11]. These events come from the Pan-STARRS1, CfA1-4, CSP, PS1, SDSS, SNLS and HST SN surveys. For the curve fitting, they used the

following formula [62]

$$\mu = m_B - M + \alpha x_1 - \beta c + \Delta_M + \Delta_B, \tag{2.5}$$

where μ is the distance modulus, m_B is the relative magnitude in the B passband, Δ_M a distance correction based on the host galaxy mass of the SN, Δ_B a distance correction based on predicted biases from simulations, α is a relation coefficient between luminosity and stretch x_1, β a relation coefficient between luminosity colour c. Finally, M is the fiducial absolute magnitude in the B passband for $x_1 = 0, c = 0$. All these correction factors are required to work with SNeIa as standard candles. We can then write

$$\mu_{\text{observational}} = m'_B - M, \tag{2.6}$$

where the corrected relative magnitude m'_B is

$$m'_B = m_B + \alpha x_1 - \beta c + \Delta_M + \Delta_B. \tag{2.7}$$

After calibrating the value for M, we can constrain the cosmological parameters of a given model by minimising the χ^2

$$\chi^2 = \frac{1}{2}\Delta\boldsymbol{\mu}^T \cdot C^{-1} \cdot \Delta\boldsymbol{\mu}, \tag{2.8}$$

where $\Delta\boldsymbol{\mu} = \boldsymbol{\mu}_{\text{observational}} - \boldsymbol{\mu}_{\text{theoretical}}$ is the difference vector between the observational distance modulus and the theoretical one. Also, C is the covariance matrix of the data that includes the statistical and systematic errors.

2.1.2 The Pantheon+ Catalogue

The Pantheon+ catalogue is an update to the previous one. It is a compilation of 1701 SNeIa [13]. It includes events at $z < 0.01$, which is a range not explored by Pantheon. The events are located in the redshift range $0.001 \leq z \leq 2.26$ [63]. All the SNeIa come from 18 different samples with 6 new large samples added in comparison to Pantheon [13]. These are the Foundation Supernova Survey [64], the Swift Optical/Ultraviolet Supernova Archive[1], the first and second samples from the Lick Observatory Supernova Search [65, 66], and the Dark Energy Survey [67]. All of these except for the Dark Energy Survey are low-redshift surveys.

[1] `https://pbrown801.github.io/SOUSA/`

Thus, they caused a large enhancement in low-redshift data on Pantheon+ in comparison with Pantheon. In this catalogue, the light curve fitting is given by [13]

$$\mu = m_B - M + \alpha x_1 - \beta c - \delta_{\mu-\text{bias}}, \tag{2.9}$$

where $\delta_{\mu-\text{bias}}$ is the bias correction derived from simulations. It is required to account for selection effects and other problems in determining the distance. The remaining parameters are the same as those for the Pantheon catalogue. As before, to constrain the cosmological parameters, we need to minimize the χ^2 function given by (2.8).

2.2 Baryon Acoustic Oscillations (BAO)

The existence of inhomogeneities in the Universe is crucial to allow the formation of structure. They allow matter to group in galaxies, and clusters of galaxies. They are caused by small perturbations. They just need to be small and appear on small scales. This enables the Universe to still fulfil the Cosmological principle on large scales. We can define two spacetimes. The background one and the physical one. The background spacetime follows the Friedmann equations and the physical spacetime describes the real Universe, with matter structure. The difference in the metric tensor between them is defined as the perturbation. However, both spacetimes are defined in different manifolds and their coordinate systems are defined with different charts. Thus, to make the difference between the metric tensor meaningful, we need to define a mapping from one spacetime to the other. It is possible to relate a point x of the physical spacetime with a point $\bar{x}$ in the background spacetime. This is done with a mapping $x = \phi(\bar{x})$. By doing so, we perform a *gauge* choice. This finally enables us to define perturbations as the difference of a quantity between the physical and the background spacetime [68, 69]. We can define the temperature perturbations as

$$\delta T = T - \bar{T}, \tag{2.10}$$

and the density perturbations

$$\delta\rho = \rho - \bar{\rho}, \tag{2.11}$$

and it is also useful to define fractional perturbations

$$\delta_\rho = \frac{\delta\rho}{\bar{\rho}}, \tag{2.12}$$

and

$$\delta_T = \frac{\delta T}{\bar{T}}, \tag{2.13}$$

where we are taking the ratio of the perturbation with the background value. We can also define the metric perturbations in the Newtonian gauge [29]

$$g_{\mu\nu} = a^2(\eta) \begin{pmatrix} -(1+2\Psi(\eta,\mathbf{x})) & 0 \\ 0 & (1+2\Phi(\eta,\mathbf{x}))\delta_{ij} \end{pmatrix}, \tag{2.14}$$

where Ψ and Φ are scalar perturbations and η is the conformal time

$$\eta(t) = \int_0^t \frac{dt'}{a(t')}. \tag{2.15}$$

The scalar perturbations satisfy the conditions $|\Psi| << 1$ and $|\Phi| << 1$. In the context of large-scale structures, these scalar perturbations play the role of perturbed gravitational potentials. The time when photons decouple from Baryons occurred approximately 380,000 years after the Big Bang. At this point, photons stopped interacting with Baryons and they started travelling freely. Those photons constitute the CMB nodaways. We can derive the density contrast differential equation by perturbing equation (1.9) and working with the 00 and spatial components. They give us the continuity and Euler equations. By breaking the coupling between them, taking the Fourier transform and assuming that we have Baryonic matter, we get [70, 71]

$$\delta_b'' + \frac{R}{1+R}\delta_b' + k^2 c_s^2 \delta_b = -k^2\Psi - 3\frac{R}{1+R}\Phi' - 3\Phi'', \tag{2.16}$$

where k is the Fourier wave number, c_s is the sound speed and R is the photon-Baryon ratio

$$R = \frac{4\bar{\rho_b}}{3\bar{\rho_\gamma}}, \tag{2.17}$$

and the prime $'$ refers to derivatives with respect to the conformal time η. Equation (2.16) describes the evolution of a single Fourier mode. It is valid in tight coupling approximation where photons and Baryons interact via Compton scat-

tering. The sound speed can be written as [70, 71]

$$c_s = \frac{c}{\sqrt{3(1+R)}}, \tag{2.18}$$

with c the speed of light. Equation (2.16) is a damped forced harmonic oscillator. The right-hand side gives the force term in terms of the scalar field perturbations and their derivatives. Physically, we have a photon-baryon fluid. Two interactions act on Baryons: pressure forces from the Compton scattering and gravitational potentials. These are the two interactions that produce the Baryon Acoustic Oscillations (BAO) and their equation is given in terms of (2.16). These waves can propagate in the fluid. Baryonic matter propagates in oscillatory motion given by [70, 72]

$$\delta_b(\eta) = \delta_{b0}\cos(kc_s\eta), \tag{2.19}$$

where δ_{bi} is the density contrast at an initial time η_i. This solution is valid when R is a constant and in the absence of gravitational potentials. Equation (2.19) has two limits. The constant regime happens for $kc_s\eta << 1$. In contrast, the oscillatory regime occurs for $kc_s\eta >> 1$. The distance travelled by the propagation is given by the sound horizon [72]

$$r_d \equiv a\int_{t_i}^{t} dt'\,\frac{c_s}{a} = a\int_{\eta_i}^{\eta} d\eta' c_s. \tag{2.20}$$

If we assume that the sound horizon is constant

$$r_d \approx ac_s(\eta - \eta_i), \tag{2.21}$$

and then we can rewrite the constant regime case when $\lambda >> d_s$ where $\lambda = (2\pi a)/k$ is a physical wavelength. So, the oscillatory case occurs for $\lambda << d_s$. Therefore, modes start to oscillate when the physical wavelength is smaller than the sound horizon.

The propagation ends when photons and Baryons decouple. This happens because of the combination of the gravitational potentials and the pressure force given by the Compton scattering. After recombination, Compton scattering stops occurring and then gravity is the only interaction that acts upon Baryons. After decoupling, BAOs get frozen in the CMB and they continue moving following the Universe expansion [70]. Nowadays, we can observe spherical shells like the ones

in[2].

In the last chapter and last section, we talked about standard candles and how they are useful for constraining cosmological parameters. We will now talk about standard rulers and how BAOs constitute standard rulers. Standard rulers are objects with a given intrinsic absolute size. Thus, if we derive the distance to a given standard ruler, we can derive the corresponding one for other standard rulers. For standard candles, we have to calibrate the absolute magnitude to be able to measure the distances and also to constrain the Hubble constant H_0. Meanwhile, for standard rulers, we need to calibrate the intrinsic size to be able to measure these quantities.

The comoving radius of a circular standard ruler r, the transverse comoving distance D_M and the angular scale θ are related by

$$\tan\theta = \frac{r}{D_M}, \tag{2.22}$$

if $\theta << 1$, then $\tan\theta \approx \sin\theta \approx \theta$. Thus,

$$\theta = \frac{r}{D_M}, \tag{2.23}$$

also, since r is the same for all standard rulers

$$D_{M2} = D_{M1}\frac{\theta_1}{\theta_2}, \tag{2.24}$$

where the subindex 1 refers to a given standard ruler and 2 refers to another one. Thus, if we determine the size of the ruler r, we can determine the distances to all of them. Now, we will focus on explaining why BAOs constitute standard rulers, or more formally statistical standard rulers [71].

Statistical standard rulers refer to objects or phenomena that have a specific known scale. Thus, it is a distribution with a characteristic scale that can be recovered statistically [71]. As we mentioned, the BAOs stopped the oscillation in the surface of the last scattering and then they entered the constant regime. Thus, in the comoving coordinates, they remained frozen after the decoupling of photons and Baryons. This is why the sound horizon provides a standard ruler.

[2] `https://apod.nasa.gov/apod/ap140120.html`

BAOs provide a preferred clustering scale given by the sound horizon.

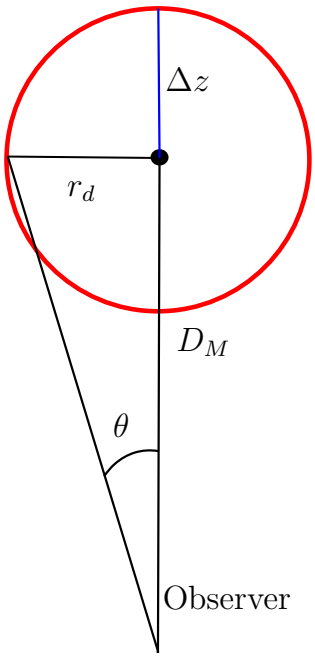

Figure 2.2: Representation of a BAO standard ruler. The red circle represents the circular clustering shells. Its radius is the sound horizon.

We plot the representation of a BAO as a standard ruler in figure 2.2. The observer is located at the bottom of the figure. From there, we observe a circular clustering shell. The distance from the observer to the centre of this circle is the angular diameter distance. The radius is the sound horizon. By measuring the angular scale, we determine the ratio

$$\theta \approx \frac{r_d}{D_M}, \tag{2.25}$$

where the approximation is very accurate for $r_d << D_M$ which is the case in cosmological distances. Furthermore, we can derive another ratio from this observation. Starting from the expression for the comoving distance (1.36), if we consider a small redshift difference Δz, and we assume that the Hubble factor is constant in this redshift difference, which is a good approximation as long as Δz is small, then

$$\Delta D_C \approx \frac{c\Delta z}{H(z)}, \tag{2.26}$$

where ΔD_C is the difference in comoving distance given by the redshift difference Δz. If this redshift difference corresponds to the blue line in figure 2.2, then the

corresponding comoving distance is the sound horizon, thus

$$\Delta z = \frac{r_d H(z)}{c}, \tag{2.27}$$

and then if we measure the redshift difference of the clustering circle, we determine the product $r_d H(z)$. Therefore, we can measure two quantities from these clustering circles: the ratio $r_d/D_M(z)$ and the product $r_d H(z)$. If we could determine r_d, we would measure D_M and $H(z)$.

We will now explore the degeneracy between r_d and H_0. This is similar to the one between M and H_0 for standard candles. We take the expression (2.25) and substitute the integral for the angular diameter distance (1.38)

$$\theta_{\rm BAO} = \frac{(1+z) r_d H_0}{c \int_0^z \frac{dz'}{E(z')}}, \tag{2.28}$$

where $E(z)$ is the adimensional Hubble factor $E(z) = H(z)/H_0$. Thus, as we can see, from the measured angular scale of clustering, we cannot determine both r_d and H_0 but just their product $r_d H_0$. Suppose we are interested in constraining one of these. In that case, we can either use an independent constraint of H_0 to measure r_d or to assume a cosmological model, compute the sound horizon with equation (1.51) and then measure H_0. The situation is similar for the redshift difference measurements

$$\Delta z_{\rm BAO} = \frac{r_d H_0 E(z)}{c}, \tag{2.29}$$

we can again only determine the product $r_d H_0$ but not them independently. We will close this section by describing the BAO catalogues that we will use in the analyses of this thesis.

2.2.1 DESI BAO 2024

This is a compilation with 5.7 million unique galaxies and quasars in the redshift range $0.1 < z < 2.1$ [14] and 420 000 Lyα forest spectra and their correlation with the spatial distribution of more than 700 000 quasars [15]. These results are part of the Dark Energy Spectroscopy Instrument (DESI)[3]. They provided results for 9 different distances. For all of them, they included the derived measurement

[3] https://www.desi.lbl.gov/

D_V/r_d where

$$D_V(z) = \left(zD_M^2(z)D_H(z)\right)^{1/3}, \tag{2.30}$$

where D_M is the comoving angular diameter distance

$$D_M(z) = (1+z)D_A(z), \tag{2.31}$$

and D_H is the Hubble distance

$$D_H(z) = \frac{c}{H(z)}. \tag{2.32}$$

The effective redshifts are $z_{\text{eff}} = \{0.30, 0.51, 0.71, 0.92, 0.93, 0.95, 1.32, 1.49, 2.33\}$ corresponding to the tracers: BGS, LGR1, LGR2, LGR3, LGR3+LGR1, ELG1, ELG2, QSO [14] and Lyman-α [15].

In addition to measuring the ratios D_V/r_d, they also provided the ratios D_M/r_d and D_H/r_d for the LRG1, LRG2, LRG3, LRG3+LRG1, ELG2 and Lyman-α tracers.

Tracer	z_{eff}	D_M/r_d	D_H/r_d	r_{off}
LRG1	0.51	13.62 ± 0.25	20.98 ± 0.61	−0.445
LRG2	0.71	16.85 ± 0.32	20.08 ± 0.60	−0.420
LRG3	0.92	21.81 ± 0.31	17.83 ± 0.38	−0.393
LRG3+LRG1	0.93	21.71 ± 0.28	17.88 ± 0.35	−0.389
ELG2	1.32	27.79 ± 0.69	13.82 ± 0.42	−0.444
Lyman-α	2.33	39.71 ± 0.95	8.52 ± 0.17	−0.480

Table 2.1: BAO distance ratios for the DESI collaboration. We include the tracers having a determination of D_M/r_d which will be used for comparison with reconstructed BAO ratios with Pantheon+. We also included the ratio D_H/r_d and the correlation between D_M/r_d and D_H/r_d, r_{off}.

In table 2.1, we included the results for the six BAO determinations of DESI including a measurement of D_M/r_d.

Chapter 3

Model-independent Comparison of SNeIa and Strong Lensing

This chapter will be based in [10]. However, we will present a difference in the analyses and results. We will calibrate the SNeIa with the most recent result of the Hubble constant from the SH0ES collaboration of $H_0 = 73.04 \pm 1.04\,\mathrm{km/s/Mpc}$ [1] rather than the one of $H_0 = 74.03 \pm 1.42\,\mathrm{km/s/Mpc}$ from [48]. This constitutes an update from the most recent result of the Hubble constant for the distance-ladder method. Furthermore, we will replace the Pantheon [11] catalogue with Pantheon+ [13]. Thus, starting from the codes used in [10], we will modify them to change the Pantheon to the Pantheon+ catalogue and also change the calibration of the SNeIa data using the last H_0 value from the SH0ES collaboration [1].

As we were saying, one way to study whether the Hubble constant tension has a physical or systematic nature is to do consistency model-independent tests. One way to do it is to work in a prediction of strong lensing results starting from SNeIa. If we do it in a model-independent way and both results are consistent, it would mean that the systematic errors from the cosmic distance ladder are smaller than the current discrepancy between SH0ES 2022 [1] and Planck 2018 [2]. The other possibility is that both SNeIa and strong lensing results are affected by the same systematics in the same way. This possibility is unlikely but cannot be ruled out by this consistency test [10]. As a further consistency check, we will repeat these analyses in the next chapter but will predict Baryon Acoustic Oscillation (BAO) results instead of strong lensing ones. This will provide further evidence on whether the Hubble tension has a physical or systematic origin.

The procedure to perform the consistency check is to start from the corrected relative magnitudes from Pantheon+ [13]. Then, the next step is to calibrate them with the absolute magnitude given by the H_0 value of SH0ES 2022 [1]. However, we do not have measurements of the relative magnitudes for all redshifts, particularly for the redshifts corresponding to the strong lensing measurements. We solve this problem by performing a Gaussian process which enables us to predict the distance modulus for any given redshift. After this, we compute the luminosity distance and from these results, we predict the strong lensing results. We describe the procedure that we will follow

1. We describe the Strong Lensing Time Delay data and convert it to Gaussian by computing the logarithm.

2. We calibrate the Pantheon+ data with the last result of H_0 from the SH0ES collaboration [1]. We also generate a binned catalogue. Finally, we run an MCMC assuming ΛCDM to verify that we are getting consistent results.

3. We read the strong lensing data and perform an MCMC test to see whether we get the expected results.

4. We perform the Gaussian process to get a continuous version of the Pantheon+ catalogue. we perform an MCMC assuming ΛCDM and compare it to the results with the full and binned Pantheon+ catalogue.

5. We use the Gaussian process predictions to derive the strong lensing distances and we make several tests comparing this data with the strong Lensing data.

We will start this chapter by describing the strong lensing results.

3.1 Strong Lensing Time Delay Measurements

Strong lensing also enables us to measure the Hubble constant H_0 [12]. Let us consider a source emitting rays towards us. Let us also assume, that during the path of the photons towards the Earth, they interact with a mass. This mass acts as a gravitational lens. Thus, different photons emitted from the source will take different paths and go over different gravitational potentials. Thus, if we have several light rays emitted from the source at the same time, they arrive at

different times at the observation point. If we consider a variable source, the time delay between multiple images can be measured by observing the lens and spotting the flux variations coming from the same source [12]. The time delay is linked to the time delay distance $D_{\Delta t}$ and it depends on several factors. These are the mass distribution of the lens, the mass distribution along the line of sight and the cosmological parameters [73, 74, 75]. The main objects that act as lenses are quasars because of their strong brightness and variable nature [76, 77, 78].

Let us consider a plane where the lens is located. The excess time delay of a picture at angular position $\boldsymbol{\theta} = (\theta_1, \theta_2)$ and source angular position $\boldsymbol{\beta} = (\beta_1, \beta_2)$ is given by [12]

$$t(\boldsymbol{\theta}, \boldsymbol{\beta}) = \frac{D_{\Delta t}}{c} \left(\frac{(\boldsymbol{\theta} - \boldsymbol{\beta})^2}{2} - \Psi(\boldsymbol{\theta}) \right), \tag{3.1}$$

where $D_{\Delta t}$ is the time delay distance and $\Psi(\boldsymbol{\theta})$ is the lens potential. This is the time delay with respect to the case of no lensing. Now, the time delay distance is given by [79, 80, 81]

$$D_{\Delta t} = (1 + z_d) \frac{D_l D_s}{D_{ds}}, \tag{3.2}$$

where z_d is the lens redshift, D_s the angular diameter distance to the source, D_l the angular diameter distance to the lens and D_{ls} the angular diameter distance between the lens and the source. As we can see, the time delay distance is inversely proportional to the Hubble constant H_0.

Let us assume that the source and the lens are closely aligned. Then, we can get multiple pictures from the same source. Then, the light rays coming from different pictures will reach the observer with different time delays. We can define the time delay difference between two pictures as [12]

$$\Delta t_{ij} = \frac{D_{\Delta t}}{c} \left(\frac{(\boldsymbol{\theta}_i - \boldsymbol{\beta})^2}{2} - \Psi(\boldsymbol{\theta_i}) - \frac{(\boldsymbol{\theta}_j - \boldsymbol{\beta})^2}{2} + \Psi(\boldsymbol{\theta}_j) \right), \tag{3.3}$$

where $\boldsymbol{\theta}_i$ and $\boldsymbol{\theta}_j$ are the positions of both pictures.

We worked with the results from the H0LiCOW collaboration[4] (H0 Lenses in COSMOGRAIL's Wellspring) [12]. We summarize the results in table 3.1. With this strong lensing data, the H0LiCOW collaboration measured a value of the Hubble constant of $H_0 = 73.3^{+1.7}_{-1.8}\,\mathrm{km/s/Mpc}$ [12] which is consistent with the last result from the SH0ES collaboration [1] but in 3.1σ tension with Planck

[4] `https://shsuyu.github.io/H0LiCOW/site/`

Lens name	Reference	z_d	$D_{\Delta t}$ (Mpc)	D_l (Mpc)
B1608+656	[81, 82]	0.630	5156^{+296}_{-236}	1228^{+177}_{-151}
RXJ1131-1231	[83, 84]	0.295	2096^{+98}_{-83}	804^{+141}_{-112}
HE0435-1223	[84, 85]	0.454	2707^{+183}_{-168}	———
SDSS1206+4332	[86]	0.745	5769^{+589}_{-471}	1805^{+555}_{-398}
WFI2033-472	[87]	0.657	4784^{+399}_{-248}	———
PG1115+080	[84]	0.311	1470^{+137}_{-127}	697^{+186}_{-144}

Table 3.1: Measured time delay $D_{\Delta t}$ and lens distances D_l with their corresponding uncertainties in the 16th and 84th percentiles. These are the results used by the H0LiCOW collaboration to measure the Hubble constant H_0.

2018 [2]. These results assume a ΛCDM model and thus are model-dependent. Therefore, strong lensing gives more evidence of the need for an alternative standard Cosmology model. The standard model gives two inconsistent results in the early and late Universe. However, the tension is still under 5σ but it adds more evidence to the hypothesis that the Hubble constant tension has a physical origin.

As we can see in table 3.1, the measurements of the time delay and lens distances are not Gaussian. We can see it since their upper and lower uncertainties are not the same. This non-gaussianity comes from the definition of the estimated distances. They come from ratios of well-measured quantities. However, if we take the logarithmic distances, they will come from sums and differences between Gaussian quantities. Thus, the distribution of the logarithm of the distances will be close to a Gaussian [10]. To derive the standard deviation and mean value of the logarithmic distances we start from the H0LiCOW data in table 3.1. The uncertainties correspond to the 16% and 85% C.L. constraints. Let us assume that we have two constraints v_1 and v_2 at two different confidence levels p_1 and p_2. If these correspond to a random variable X, the mean value $\mu(\log_{10} X)$ and the variance $var(\log_{10} X)$ are given by [10]

$$\mu(\log_{10} X) = -\frac{\mathrm{Erf}^{-1}(2p_2 - 1)|\log_{10} v_1 - \log_{10} v_2|}{|\mathrm{Erf}^{-1}(2p_2 - 1) - \mathrm{Erf}^{-1}(2p_1 - 1)|}, \tag{3.4}$$

$$var(\log_{10} X) = \frac{\log_{10} v_1 - \log_{10} v_2}{\sqrt{2}|\mathrm{Erf}^{-1}(2p_1 - 1) - \mathrm{Erf}^{-1}(2p_2 - 1)|}, \tag{3.5}$$

where Erf^{-1} is the inverse error function.

Lens name	z_d	$\log_{10}(D_{\Delta t}/\text{Mpc})$	$\log_{10}(D_l/\text{Mpc})$
B1608+656	0.630	3.714 ± 0.022	3.090 ± 0.058
RXJ1131-1231	0.295	3.323 ± 0.019	2.908 ± 0.068
HE0435-1223	0.454	3.433 ± 0.028	——
SDSS1206+4332	0.745	3.758 ± 0.032	3.261 ± 0.113
WFI2033+472	0.657	3.686 ± 0.029	——
PG1115+080	0.311	3.167 ± 0.039	2.844 ± 0.102

Table 3.2: Logarithmic time delay $\log_{10}(D_{\Delta t}/\text{Mpc})$ and lens $\log_{10}(D_l/\text{Mpc})$ distances with their corresponding uncertainties at 1σ C.L. These results were computed from expressions (3.4) and (3.5).

3.2 SNeIa data

After describing the strong lensing data, we perform some checks on the SNeIa data from Pantheon+ [13]. The Pantheon+ collaboration provides measurements of the corrected relative magnitude m'_B. However, the covariance matrix works for the distance modulus instead of the relative magnitude. Thus, we need to calibrate it with the absolute magnitude M or taking a value of H_0 and constraining M. As we have mentioned, calibrating M with cepheid variable stars is the way to measure H_0 [1]. Here, we will calibrate M in a way that the corresponding mean value of H_0 will be the one of the SH0ES collaboration $H_0 = 73.04$km/s/Mpc. We start from a fiducial value M_{fid} corresponding to $H_0 = 70$km/s/Mpc [88]. This gives $M_{\text{fid}} = -19.3$. The difference between this fiducial value and the observed one is [10]

$$M - M_{\text{fid}} = 5\log_{10}\left(\frac{H_0}{H_{0\,\text{fid}}}\right), \tag{3.6}$$

and in this case $M = -19.21$. Moreover, the covariance has to also take into account the uncertainty of the determination of H_0. For the result that we are considering, $\sigma_{H_0} = 1.04\,\text{km/s/Mpc}$. The new covariance is given by [10]

$$cov(\mu)_{ij} = cov(\mu_{\text{fid}})_{ij} + \left(\frac{5}{\ln 10}\frac{\sigma_{H_0}}{H_0}\right)^2, \tag{3.7}$$

where $\mu_{\text{fid}} = m - M_{\text{fid}}$ and $\mu = m - M$. The indices i, j run over all the SNeIa catalogue.

To check that our implementation works, we performed an MCMC with the calibrated data. We computed the theoretical distance modulus with the equation (2.4). Moreover, the Hubble factor for ΛCDM is given by (1.33), which has two

parameters $\Theta = \{H_0, \Omega_m\}$. To perform the MCMC, we used the `PyMultiNest`[5] software [89]. Finally, it is important to notice that to infer distances from the SNeIa data, we need to apply a small correction and convert between the heliocentric and the CMB reference frames. Thus, we need to correct the heliocentric redshift z_h to the CMB redshift z_{CMB} [10]

$$5\log_{10}\left(\frac{D_L(z_{CMB})}{10\,\mathrm{pc}}\right) = m - M - 5\log_{10}\left(\frac{1+z_h}{1+z_{CMB}}\right). \tag{3.8}$$

While the Pantheon data includes a binned version, Pantheon+ does not include it. A binned version of the data allows us to perform analyses with much lower computational time and give very similar results. Thus, we built a binned version of Pantheon+. We ran several analyses to determine the best number of bins that we needed, which turned out to be 55. We divided the Pantheon catalogue into this number of bins with the same number of events in each one. We derived the mean value, uncertainties and covariance matrix of the binned data. Finally, we performed the MCMC with both the full and binned Pantheon+ catalogue.

We present the marginalized posterior in figure 3.1 for the full Pantheon+ and the binned Pantheon+ catalogues. Furthermore, we include the result from SH0ES 2022 [1] which was the value that we used for the calibration. As we can see, the posterior is very similar to the binned Pantheon+ having a slightly bigger uncertainty and contours. However, the confidence regions of the binned Pantheon+ catalogue lie within the ones for the full Pantheon+. Thus, the binned catalogue predicts the same cosmological results with slightly bigger uncertainties. This will be important for the next analyses. In addition to this, we see that both catalogues are consistent with the H_0 result from the SH0ES collaboration [1]. This was a requirement since we calibrated the data using this result.

Catalogue	H_0 (km/s/Mpc)	Ω_m
Full Pantheon+	73.0 ± 1.1	0.341 ± 0.028
Binned Pantheon+	72.8 ± 1.2	0.346 ± 0.038

Table 3.3: Mean values along with the 1σ C.L. uncertainties for the full and binned Pantheon+ catalogues. We assumed the ΛCDM model and a calibration of H_0 using the value of $H_0 = 73.04 \pm 1.04\,\mathrm{km/s/Mpc}$ from the SH0ES collaboration [1].

We included the results for the mean values and uncertainties at 1σ C.L. in

[5] `https://github.com/JohannesBuchner/PyMultiNest`

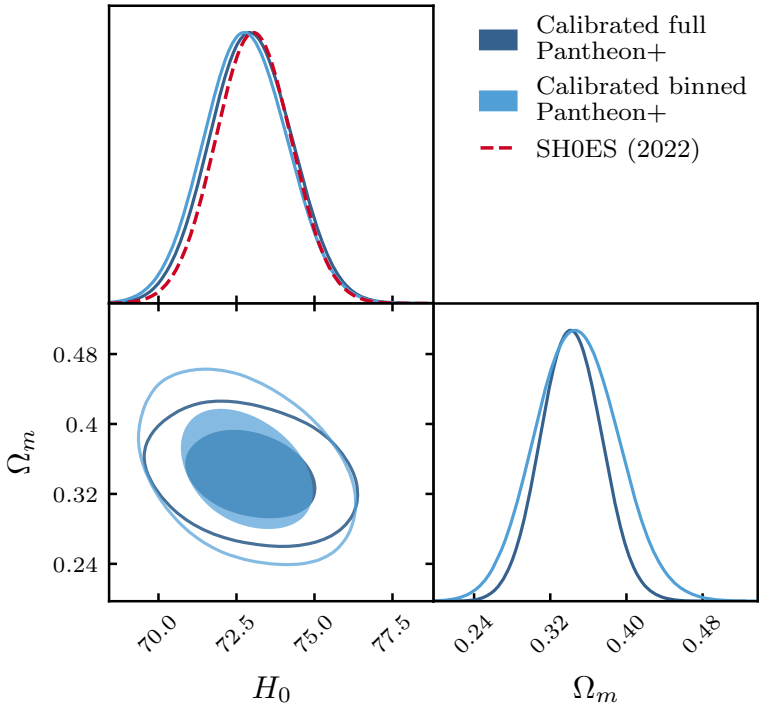

Figure 3.1: Marginilized posterior for the ΛCDM model and the full Pantheon+ and binned Pantheon+ catalogues. We also included the SH0ES 2022 result of H_0 to check that the calibration is accurate. We included the 1σ and 2σ C.L. confidence contours.

table 3.3. As we can see, both results are consistent with the calibration and the binned catalogue has a slightly bigger uncertainty for the matter content Ω_m.

3.3 Strong Lensing Constraints

We have verified that the SNeIa data works as it should. We checked this by calibrating the data and fitting it using the standard ΛCDM model. In this section, we report the results by fitting the strong lensing data to the ΛCDM model using the logarithmic data.

Baseline	H_0 (km/s/Mpc)	Ω_m
Time delay distance	73.0 ± 1.3	$0.25^{+0.13}_{-0.16}$
Lens distance	$81.6^{+8.2}_{-9.1}$	$0.22^{+0.077}_{-0.22}$

Table 3.4: Mean values along with the 1σ C.L. uncertainties for the time delay and lense distances. We assumed the standard ΛCDM model.

We present the confidence contours in figure 3.2. Our analyses give the same results as in [10] and are also consistent with the results from the HoLiCOW

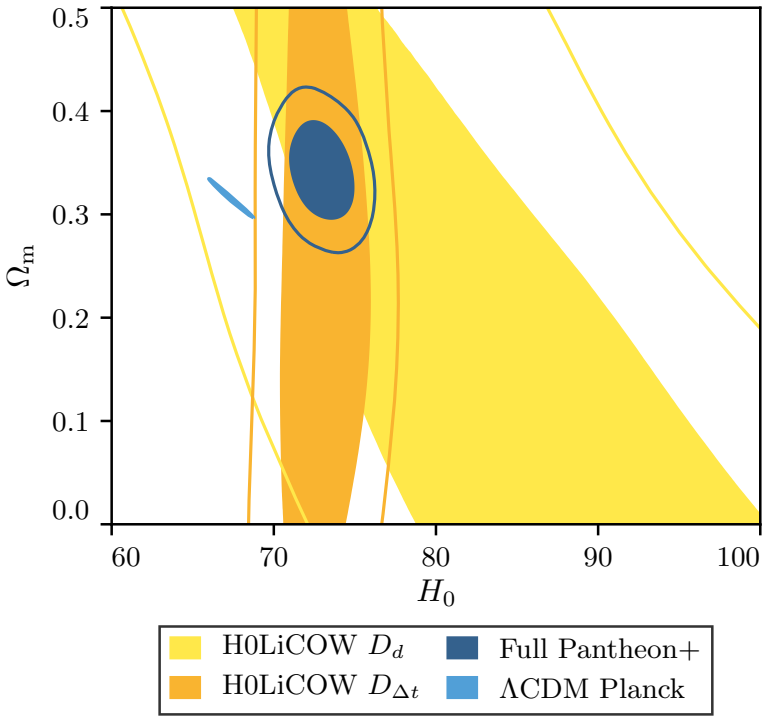

Figure 3.2: Confidence contours at 1σ and 2σ C.L. for the strong lensing data and the ΛCDM model. We included the results from the full Pantheon+ catalogue and Planck 2018 [2] for comparison.

collaboration [12]. We also included the results from our calibration for the full Pantheon+ catalogue and for ΛCDM Planck 2018 [2]. Also, we present the constraints in table 3.4. As we can see, the time delay measurements provide a very accurate determination of the Hubble constant H_0 which is fully consistent with the value from the SH0ES collaboration [1]. The constraint for the lens distance was higher but it is still consistent with this result at 2σ C.L. We can also note that the matter content has weak constraints. We can spot in figure 3.2 and table 3.4 that the matter content is not well constrained and can even get higher than $\Omega_m = 0.5$ or even approach $\Omega_m = 0$. We will now focus on performing the Gaussian processes.

3.4 Gaussian Process Regression on the SNeIa Data

Since we want to make a consistency check by computing the time delay and lens distances starting from the SNeIa, we need to build a continuous catalogue. The redshifts of time delays and lenses are not equal to the redshifts from the

Pantheon+ catalogue. Thus, if we want to predict the strong lens distances, we need to be able to generate SNeIa data in these redshifts. The method to perform this is to do a Gaussian Process (GP) Regression on the Pantheon+ catalogue.

The first stage is to define our timescale. When we built the Pantheon+ binned catalogue, we divided the data into 55 bins with the same amount of SNeIa events. Also, the full Pantheon+ SNeIa events are not equally spaced in Redshift. Then, if we want to guarantee that the GP recovers the relative weights of the binned catalogue, we need a unique map between uniformly spaced redshifts and the redshifts of the Pantheon+ binned catalogue. This will ensure that the GP does not establish artefacts that are a function of the distance difference between the SNeIa events. Thus, we define a new time coordinate where the Pantheon+ events are equally spaced in redshift. We will use this time coordinate to define the GP [10].

To be sure that the estimated strong lensing distances are accurate, we need to ensure that the GP has sufficient liberty to represent all the variations from the Pantheon+ catalogue. The variations in the Pantheon+ binned catalogue are tiny in comparison to the variations in the distance-redshift relation. To predict this relation with the GPs, we deduct from the Binned data the best fit of the standard ΛCDM model and we add it again after the GPs. In this way, we work with points that are dispersed around zero. The amount of flexibility of the GP is related to the chosen kernel function. These functions describe the relative correlation between distinct data with other time coordinates. We work with the three kernels used in [10]. The first one is the exponential squared kernel [90]

$$k(x_a, x_b) = \sigma^2 \exp\left(-\frac{||x_a - x_b||^2}{2\ell^2}\right), \tag{3.9}$$

where σ^2 is the overall variance, σ is called the amplitude, and ℓ is the length scale which gives the variance of the kernel. The second kernel that we consider is known as the Matern kernel of order $\nu = 9/2$. For an arbitrary ν, this kernel is given by [90]

$$k(r) = \frac{2^{1-\nu}}{\Gamma(\nu)}\left(\frac{\sqrt{2\nu}r}{\ell}\right)^{\nu} K_\nu\left(\frac{\sqrt{2\nu}r}{\ell}\right), \tag{3.10}$$

where r is the distance between the two points and can also be written as $r = ||x_a - x_b||$ and ν and ℓ are parameters. Finally, we considered the ratio-

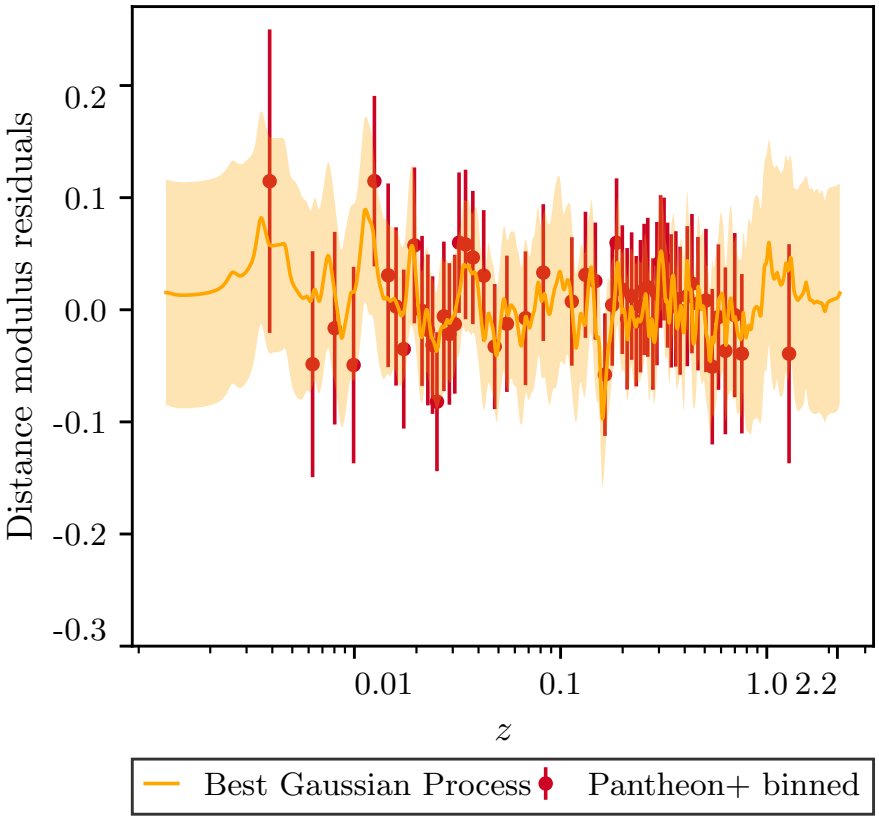

Figure 3.3: Distance modulus residuals for the binned Pantheon+ catalogue in comparison to the best GP kernel, which is the rational quadratic kernel. The GP predictions represent a continuous line with the orange line as the mean value and the light orange region as the uncertainties at 1σ C.L.

nal quadratic kernel [90]

$$k(r) = \sigma^2 \left(1 + \frac{r^2}{2\alpha\ell^2}\right)^{-\alpha}, \tag{3.11}$$

where α is a positive parameter called scale-mixture and ℓ the length scale as in the previous cases. As we can see, two of the kernels that we are considering have two parameters while the rational quadratical one has three. For the three kernels, it is required to add a constant offset similar to the one in equation (3.7). This is to correctly replicate the correlation between the SNeIa [10].

The best parameters for the kernels are computed by minimizing the Kullback-Leibler (KL) divergence [91]. The minimization is performed between the GP forecast and the binned Pantheon+ catalogue. The KL divergence constitutes the information variation between the GP and the binned Pantheon+ data. It acts as a quantification of how much the two distributions are different. For two Gaussian probability distribution functions, P_{GP} and P_d, the divergence is given by [10]

$$D(P_d|P_{GP}) \equiv \frac{1}{2\ln 2}\left((y_d - y_{GP})^T \Sigma_d^{-1}(y_d - y_{GP}) - \ln\frac{\det\Sigma_{GP}}{\det\Sigma_d} - d + tr\left(\Sigma_{GP}\Sigma_d^{-1}\right)\right), \tag{3.12}$$

where y_d and y_{GP} are the distance modulus residuals from the binned Pantheon+ data and the GP predictions for a given value of the Kernel parameters. Σ_d is the covariance matrix of the binned Pantheon+ catalogue and Σ_{GP} the covariance for the GP, which is conditioned on the full Pantheon+ catalogue and d is the number of bins in the binned Pantheon+ catalogue.

The KL divergence allows us to determine the kernel with the best performance. In our case, the optimal value kernel values are given by: the exponential squared kernel $KL = 0.844$, the Matern kernel $KL = 0.828$, the rational quadratic kernel $KL = 0.814$. Then, the latter one has the best performance. Thus, the main results from this chapter will be from this kernel.

We present a comparison of the distance modulus residuals from the binned Pantheon+ catalogue and the GP with the best kernel in figure 3.3. We can notice that the reconstructed GP distance modulus is continuous. Moreover, we can see that all the binned points lie within 1σ C.L. from the predicted distance

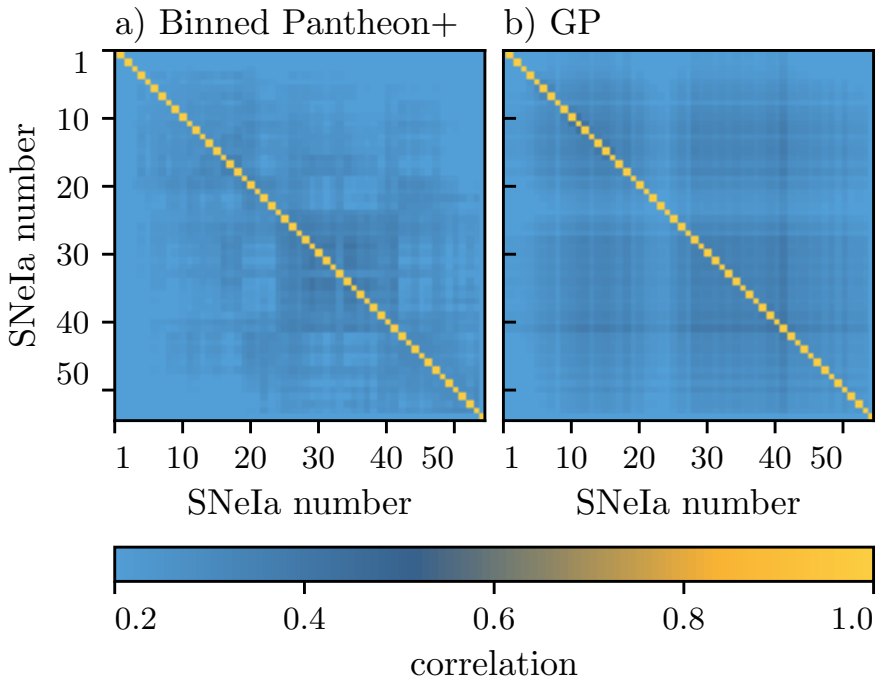

Figure 3.4: Correlation matrix for the Binned Pantheon+ catalogue and the predicted GP reconstruction.

modulus residuals from the GP. Also, most of the data points are very close to the mean values of the GP. This shows that the GP reconstruction is accurate.

We now turn our attention to see if the GP is retrieving the correlation between data close to the binned Pantheon+ catalogue. The correlation comes from calibration between SNeIa pairs and systematic errors [1, 46]. We present a visual figure showing the correlations between the SNeIa events of the binned Pantheon+ catalogue and the reconstructed catalogue using GP. We include these results of the correlation matrix in figure 3.4. As we can see, the diagonal elements have very similar results and the non-diagonal elements show a slight difference which is not very different from Figure 8 in [10].

Before moving on to the predictions of the strong lensing results using the GP, we will do a final consistency check. We will perform an MCMC with the reconstructed GP data. Thus, we will suppose that the GP reconstructions are real data and fit it to the standard ΛCDM model. We will do it in the same redshifts of the full Pantheon+ catalogue to see how similar the constraints are. This will tell us whether the reconstruction is accurately reproducing the Pantheon+

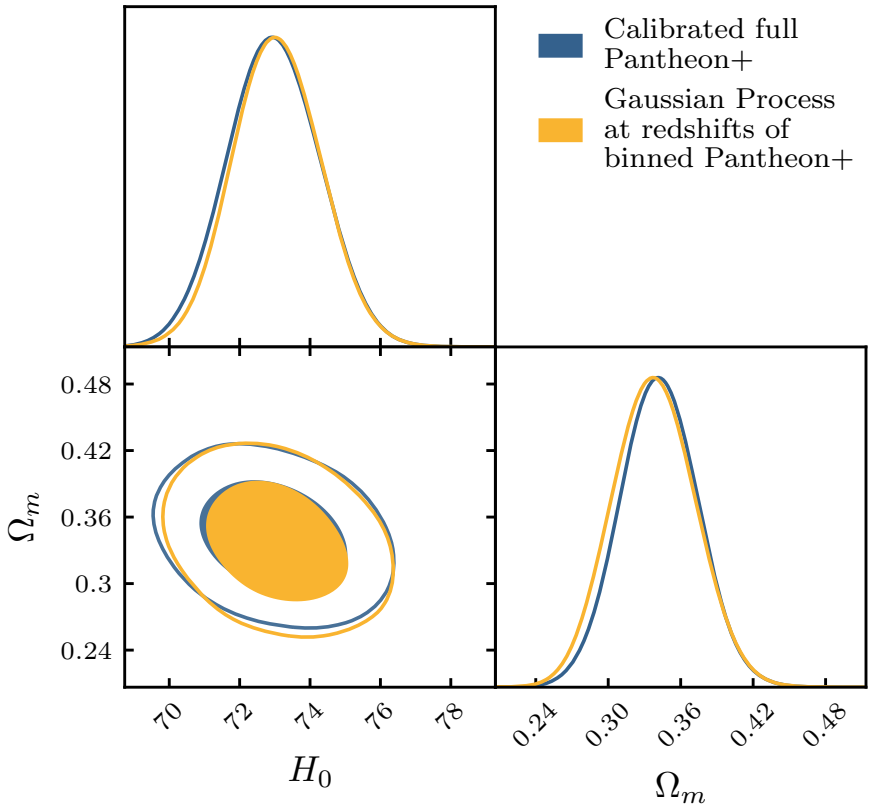

Figure 3.5: Marginilizad posterior for the ΛCDM model and the full Pantheon+ catalogue and GP reconstruction fitted at the redshift of the Pantheon+ catalogue. We include the 1σ and 2σ confidence contours.

catalogue. We show these results in figure 3.5. As we can spot, the constraints are almost identical with only slight differences. Therefore, this consistency test proves that our GP reconstruction accurately reproduces the full Pantheon+ catalogue. We can now focus on predicting the strong lensing distances using this GP reconstruction that has passed our consistency tests.

3.5 GP Reconstruction of the Time Delay and Lens Distances

After getting a continuous dataset from the GP that accurately describes the Pantheon+ catalogue, we can derive the predicted strong lensing distances. To do this, we need to predict luminosity distances from the reconstructed GP Pantheon+ catalogue. This can easily be done by solving $D_L(z)$ in equation (1.42)

$$D_L(z) = 10^{(\mu(z)+5)/5}\,\mathrm{pc}, \tag{3.13}$$

where $\mu(z)$ is the distance modulus. Thus, from the predicted GP distance modulus, we can derive the luminosity distance for any redshift. Starting from this result, we can also derive the angular diameter distance with equation (1.41). This allows the reconstruction of the angular diameter lens distances. Finally, for the time delay distances, we use equation (3.2). Therefore, we can predict the strong lensing distances starting from the GPs. Moreover, this determination is model-independent. Thus, it allows us to perform a consistency check on the SNeIa data from Pantheon+ [13] and the calibration with SH0ES 2022 [1].

We include the results of the ratio between the H0LiCOW strong lensing data and Pantheon+ GP reconstruction in figure 3.6. We included the mean values and 1σ C.L. uncertainties. In sub-figure (a), we included the comparison for the time delay distances and (b) for lens distances. As we can see, the error bars for the GP lens distance reconstruction are much smaller than the ones for H0LiCOW. The cause of this is that the reconstruction comes from a large number of SNeIa at intermediate redshift. On the other hand, the error for the GP time delay reconstruction is similar to H0LiCOW. This is due to how we compute the time delay distance which comes from the product and ratio of different random variables.

Let us remember that the logarithmic H0LiCOW data is close to Gaussian

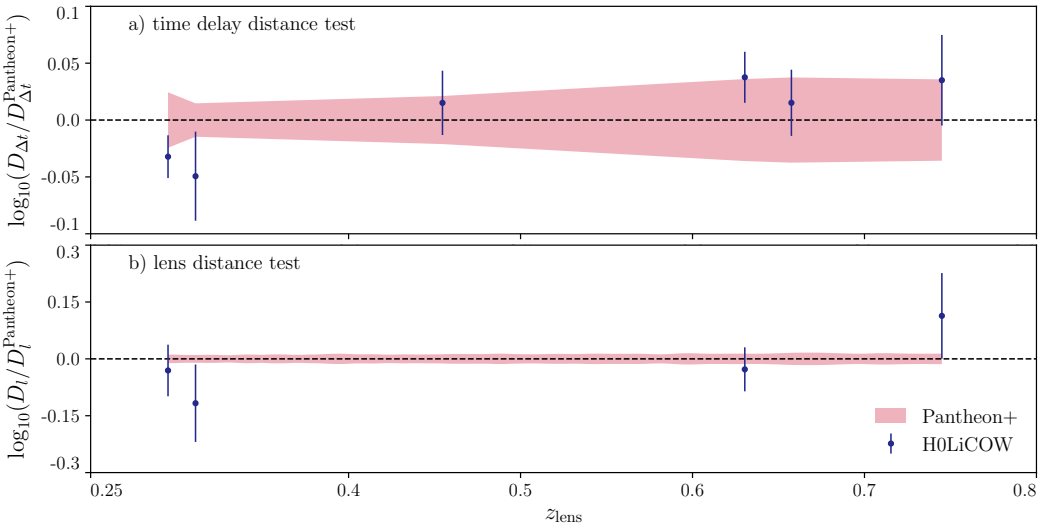

Figure 3.6: Comparison of the H0LiCOW time delay (a) $D_{\Delta t}$ and lensing (b) D_l distances with the calibrated Pantheon+ data reconstructed GP values $D_{\Delta t}^{\rm Pantheon+}$ and $D_l^{\rm Pantheon+}$. We plot the mean values for H0LiCOW along their 1σ C.L. uncertainties. For the reconstructed Pantheon+ GP, we plot the mean value at the zero ordinate coordinate and we include the 1σ C.L. confidence region in light red.

and also the GP reconstruction is close to Gaussian. Thus, we can measure the agreement with

$$\chi^2 = (\log_{10}\mathbf{D}_{\Delta t} - \log_{10}\mathbf{D}_{\Delta t}^{\rm Pantheon+})^T C_{\rm tot}^{-1}(\log_{10}\mathbf{D}_{\Delta t} - \log_{10}\mathbf{D}_{\Delta t}^{\rm Pantheon+}), \quad (3.14)$$

where $C_{\rm tot}$ is the sum of the covariance matrix of the H0LiCOW data and the reconstructed data with GP. The significance test is then given by

$$\text{significance} = 1 - \text{CDF}(\chi^2), \quad (3.15)$$

where CDF is the cumulative distribution function. The perfect agreement would mean a significance of 100%. The significance can be converted to confidence levels (C.L.) in units of sigma with the formula

$$\text{C.L.}(\sigma) = \sqrt{2}\text{Erf}^{-1}(\text{significance}), \quad (3.16)$$

where Erf is the error function. The significance (and C.L.) for the time delay distances is 68.9% (0.401σ). On the other hand, for the lens distance is 60.8%

(0.512σ). These results are different than the correspondent ones in [10] where they worked with the Pantheon catalogue and the calibration of H_0 from [48]. They got significances of 85.7% and 63.6%. The significance for the lens distance is similar but the one for the time delay distances is considerably higher. Even so, by changing the SNeIa to Pantheon+ and the H_0 calibration from [1], we still get significances way lower than 1σ C.L. This means that if the reconstructed GP were real data, they would not be in tension from the measurement of H0LiCOW. The agreement also implies that the systematics of the determination of H_0 with Pantheon+ SNeIa should be relatively small, otherwise, they would produce big biases when reconstructing the strong lensing distances. However, there is still the unlikely possibility that both Pantheon+SH0ES and H0LiCOW share the same systematics. This is one of the reasons to continue the consistency test with BAOs in the next chapter.

We have tested the amplitude of the reconstructed strong lensing distances from the GPs. However, we also need to ensure that the shape of the reconstructed curve is consistent with H0LiCOW. This amplitude test studies the possible discrepancies in the determination of H_0 while the shape test assesses whether the GP reconstruction follows the same shape without an H_0 calibration [10]. To perform the amplitude test, we need to compute the mean value of the logarithmic H0LiCOW results and the reconstructed GP ones. For the uncertainty, we compute

$$\sigma_{\text{Amplitude}} = \frac{\sum_{i=1}^{N} C_{ii}}{N^2}, \tag{3.17}$$

where N is the total number of measurements. The average amplitude of the H0LiCOW time delay distances is $\langle \log_{10} D_{\Delta t} \rangle = 3.514 \pm 0.012$. This result for the reconstructed GP data from Pantheon+ is $\left\langle \log_{10} D_{\Delta t}^{\text{Pantheon+}} \right\rangle = 3.512 \pm 0.013$. These results have a significance of 90.5% (0.12σ). On the other hand, for the lens distances, we have $\langle \log_{10} D_l \rangle = 3.026 \pm 0.044$ and $\left\langle \log_{10} D_l^{\text{Pantheon+}} \right\rangle = 3.041 \pm 0.008$. They have a significance of 73% (0.346σ). Thus, this test confirms the agreement between the H0LiCOW date and the predictions from GP and Pantheon+.

We now focus on testing the redshift dependence of the data. This can be done by computing distance ratios or the difference of logarithmic distances.

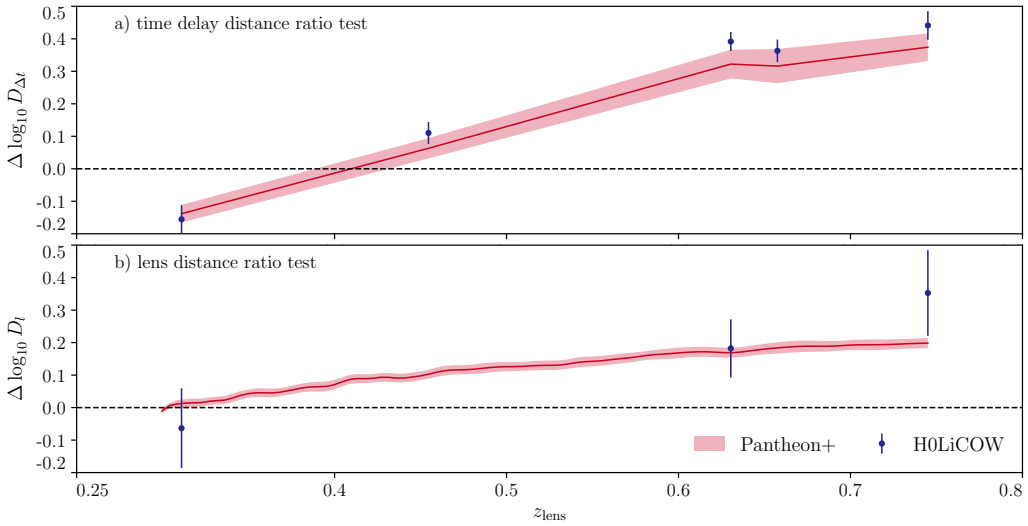

Figure 3.7: Comparison of the difference of H0LiCOW time delay (a) $\Delta D_{\Delta t}$ and lensing (b) ΔD_l distances with the calibrated Pantheon+ data reconstructed GP values $\Delta D_{\Delta t}^{\rm Pantheon+}$ and $\Delta D_l^{\rm Pantheon+}$. We plot the mean value along their 1σ C.L. uncertainties for both measurements. The difference is computed by taking the ratio of the distances with respect to the lowest lens redshift and then taking the base 10 logarithm.

Thus, since the Hubble constant is inversely proportional to the distance, it cancels when considering the ratio. We take all the measurements and take the ratio of them with respect to the one with the lowest lens redshift. This is an arbitrary election but it does not lose generality. If we change the datum to which we take the ratio, we would get a different linear combination of the data [10]. We plot these results in figure 3.7. As we can see, the results also show good agreement. The significance of this test for the time delay data is 57.4% (0.563σ) and for the lens distances is 51.3% (0.655σ). These significances are lower than the ones for the amplitude test. However, they are still way below the 1σ C.L. which implies good agreement. We summarize the results from the predicted strong lensing distances in table 3.5.

We now move to a different kind of test. This next step consists of creating simulated H0LiCOW data and repeating the previous analyses. This is done by introducing a bias on the measured distances $D_{\Delta t}$ and D_l. The mean values and covariances need to be changed to maintain the signal-to-noise ratio constant [10]. Then, we will examine the consistency between the new biased data with

Lens name	z_d	$\log_{10}\left(D_{\Delta t}^{\text{Pantheon+}}/\text{Mpc}\right)$	$\log_{10}\left(D_{l}^{\text{Pantheon+}}/\text{Mpc}\right)$
B1608+656	0.630	3.677 ± 0.036	3.118 ± 0.014
RXJ1131-1231	0.295	3.355 ± 0.025	2.938 ± 0.011
HE0435-1223	0.454	3.418 ± 0.021	——
SDSS1206+4332	0.745	3.728 ± 0.036	3.147 ± 0.014
WFI2033-4723	0.657	3.67 ± 0.037	——
PG1115+080	0.311	3.216 ± 0.015	2.961 ± 0.010

Table 3.5: Predicted time delay $\log_{10}\left(D_{\Delta t}^{\text{Pantheon+}}/\text{Mpc}\right)$ and lens $\log_{10}\left(D_{l}^{\text{Pantheon+}}/\text{Mpc}\right)$ logarithmic distances from the GP using the Pantheon+ catalogue with their corresponding uncertainties at 1σ.

Pantheon+.

We start by assuming a constant +8% shift for the time delay $D_{\Delta t}$distances and a +15% shift for the lensing distances D_l. We find that this changes the significance to 34.1% (0.952σ) and 53.6% (0.619σ) respectively. As we can see, this constant bias increases the tension between the GP reconstructed distances and the H0LiCOW data. However, it is still consistent under 1σ C.L. We also consider a redshift-dependent bias with parameter $0.5(z_{\text{lens}}-z_{\text{mean}})$ [10] with z_{mean} the mean redshift of the lenses. This changes the significance to 0.935% (2.6σ) for the time delay distances and 22% (1.23) for the lens distances. As we can see, with a bias like this, we can achieve a tension between the data and the predicted values.

Before moving on to the comparison of SNeIa and BAO, we summarize the analyses and results. These analyses provide a model-independent consistency check between strong lensing data from H0LiCOW [12] and SNeIa data from the Pantheon+ catalogue [13]. The method used the measurement of 1701 SNeIa in a big range of redshifts. The method made use of GP to interpolate between the measurements and build a continuous version of the Pantheon+ catalogue. Then, we compared the residuals, the covariance matrix and the MCMC constraints with the ΛCDM model of the newly continuous catalogue and realized that it accurately describes the full Pantheon+ baseline. After this, we converted the predicted GP distance modulus to luminosity distances and then to logarithmic lens distances $D_l^{\text{Pantheon+}}$ and time delay distances $D_{\Delta t}^{\text{Pantheon+}}$. We compared these predicted distances with the H0LiCOW measurements and found that their significance is way lower than 1σ C.L. We repeated the analysis by computing the

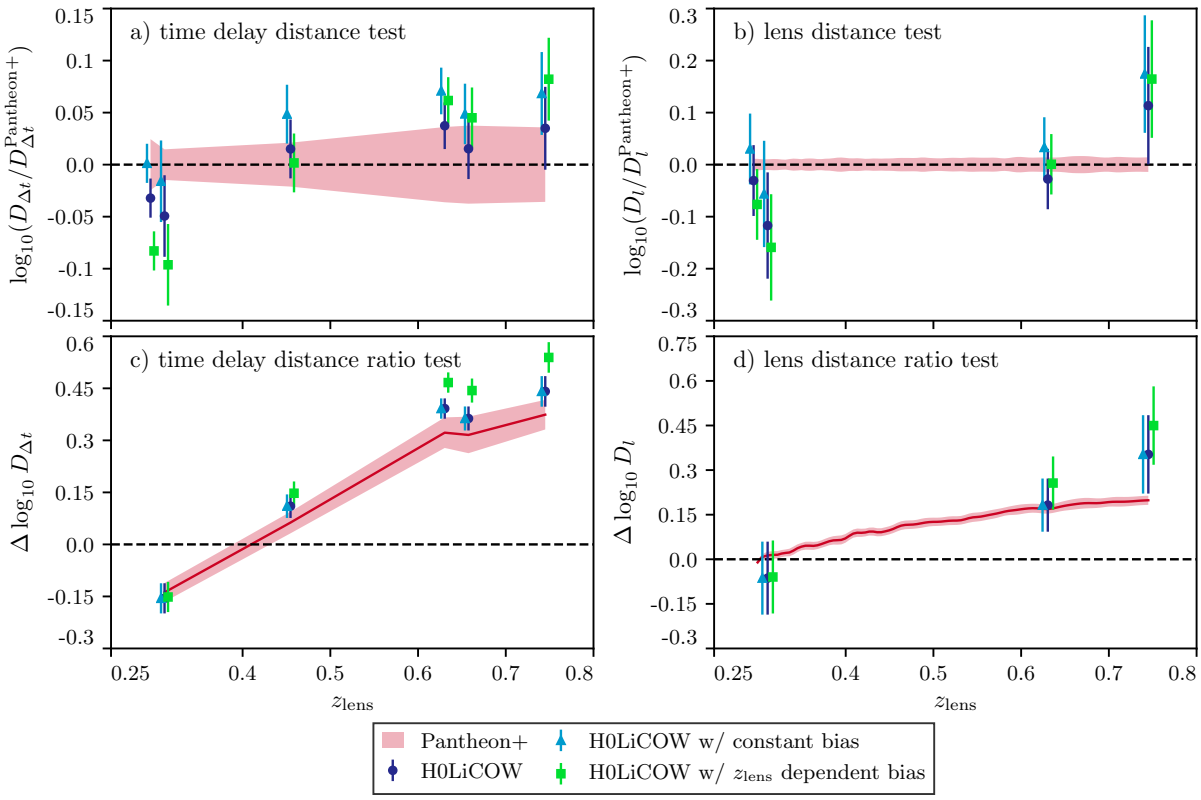

Figure 3.8: Comparison of the biased H0LiCOW data with the GP reconstructed Pantheon+ data. This figure is similar to 3.6 and 3.7 but we are introducing a +8% and a 15% constant biases to the time delay distance $D_{\Delta t}$ and lensing distance D_l respectively. Furthermore, we also include the results by introducing a redshift-dependent bias parametrized by $0.5(z_{\rm lens} - z_{\rm mean})$.

difference of logarithmic distances for all points with respect to the case with the lowest lens redshift. Once again, the significance was way lower than 1σ C.L. We also computed the overall amplitude of the measurements and found that they were also consistent. We then included a bias to the H0LiCOW data of 8% for the time delay distances and 15% for the lens distances. We found that this bias induces a disagreement between the predicted reconstructed distances and the biased H0LiCOW data. However, the significance was still always below 2σ C.L. This means that even if the strong lensing data is biased by around 15%, they are still consistent with the predicted data from SNeIa. This changed for the case of a redshift-dependent bias of the form $0.5(z_{\rm lens} - z_{\rm mean})$. We got a tension over 2σ C.L. for this bias and the time delay distances.

Therefore, since this consistency check is model-independent, there is no sign

that there are unaccounted systematic effects on both data sets. This gives more evidence to the hypothesis that a new standard model of Cosmology is needed to account for the tension between SH0ES 2022 [1] and Planck 2018 [2]. The tests performed in this chapter were both H_0 calibration-dependent (ratio between strong lensing distances and predicted SNeIa distance) and H_0 calibration-independent (difference between distances and the distance at the minimum lensing redshift). Both tests showed agreement between the H0LiCOW data and the predicted data from the Pantheon+ catalogue. However, there is still the possibility that both data sets have the same unaccounted systematic effects, of the same sign, magnitude and redshift dependence [10]. This consistency test is not sensible of this remote possibility. In the following chapter, we will repeat the reconstruction but instead of predicting strong lensing distances, we will predict BAO distance ratios. This will shed more light on the possibility that H0LiCOW and Pantheon+ data can be affected by the same systematics. If the reconstructed BAO distance ratios from Pantheon+ are consistent with BAO measurements, then this prospect would be even more unlikely and we would get more evidence for the hypothesis that the Pantheon+ catalogue is not being affected by unknown systematic errors.

Chapter 4

Model-independent Comparison of SNeIa and BAO distance ratios

In the previous chapter, we predicted the strong lensing distances of the H0LiCOW collaboration [12] from the GP reconstruction of the Pantheon+ catalogue. The analyses pointed out that since the predicted strong lensing distances are consistent with the measurements, then this shows that there is no evidence for unaccounted systematics in both methods. Even so, this consistency test cannot rule out the unlikely scenario where both distances have the same unknown systematics of the same magnitude and redshift. Thus, doing further consistency tests would enable us to discard this possibility. In this chapter, we will focus on predicting BAO distance ratios starting from the SNeIa Pantheon+ catalogue.

We have already built the reconstructed continuous version of Pantheon+, so the task here is to use this catalogue to predict a different kind of observable. We will focus on BAOs. As we mentioned, they constitute standard rulers. Furthermore, they enable a model-independent measurement of $D_M(z)/r_d$ and $(r_d H(z))/c$. Therefore, they measure two adimensional quantities. Let us recall that from the GP reconstruction of the Pantheon+ catalogue, we can predict luminosity distances. Thus, we can predict the transverse comoving distance $D_M(z)$. However, we are not able to predict the sound horizon r_d or the Hubble factor $H(z)$. Consequently, we need a calibration of the sound horizon to predict BAO distance ratios. Besides, this calibration must be model-independent. We will start this chapter on how to perform this calibration of the sound horizon r_d.

4.1 Model-independent Determination of the Sound Horizon r_d

The goal is to determine the sound horizon r_d without invoking a cosmological model [92]. The method starts by generating samples from the BAO data. We take the mean values and covariance of the ratios $D_M(z)/r_d$ and generate samples using a Gaussian distribution. So that the samples follow

$$(D_M(z)/r_d)_{\text{samples}} \sim \mathcal{N}(\mu_{\text{BAO}}, \sigma^2_{\text{BAO}}), \tag{4.1}$$

where μ_{BAO} and σ_{BAO} are the mean values and standard deviations of the BAO catalogue. After this, we generate the same number of samples from the GP reconstruction using the Pantheon+ catalogue. These samples give us the reconstructed luminosity distance. We can convert these results to transverse comoving distance by dividing by $(1+z)$. We then take the ratio

$$(r_d)_{\text{samples}} = \frac{D_M^{\text{Pantheon+}}(z)}{(D_M(z)/r_d)_{\text{samples}}}, \tag{4.2}$$

where the result depends on the redshift. This allows for the determination of the sound horizon at a given redshift. However, the sound horizon is a constant after recombination and it must be redshift-independent. We do this by converting the samples to MCMC samples and then computing the mean values and the standard deviation.

z_{BAO}	r_d (Mpc)
0.51	132.09 ± 4.46
0.706	140.59 ± 5.44
0.92	133.52 ± 6.32
0.93	134.98 ± 6.24
1.317	137.48 ± 6.70
2.33	131.88 ± 6.88
All	135.09 ± 3.47

Table 4.1: Determination of the model-independent sound horizon for each of the BAO measurements in the DESI BAO 2024 catalogue and the global determination.

For the DESI BAO 2024, we present the results of this in table 4.1 and in figure 4.1. The problem with this determination is that the predicted r_d depends

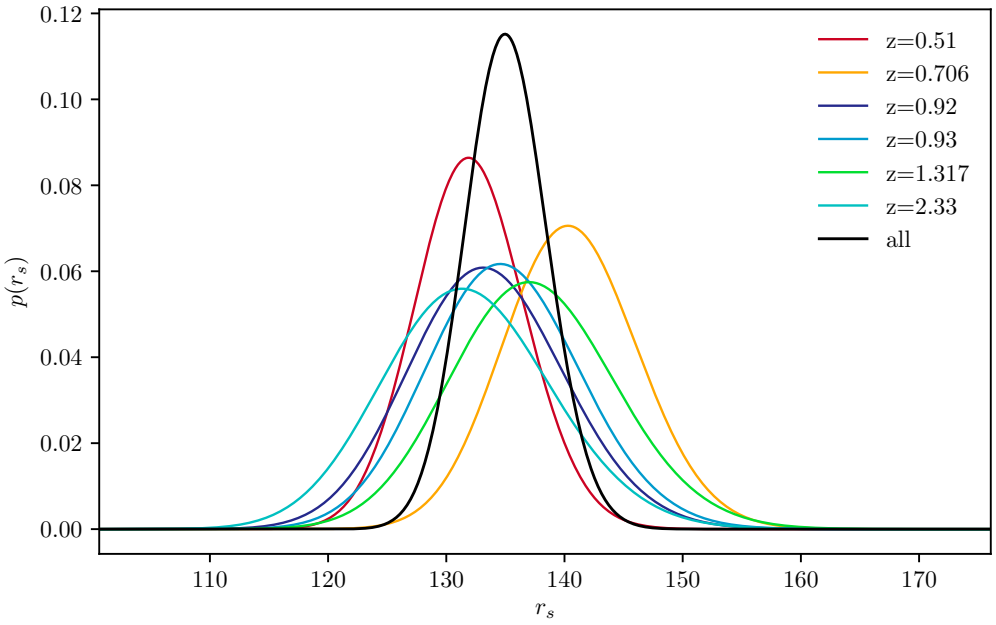

Figure 4.1: Model-independent constraints of the sound horizon r_d using the BAO DESI 2024 data [14, 15] and the reconstructed BAO Pantheon+ GP data. We present the individual constraints for each BAO measurement and the overall constraint.

on the calibration of the GP reconstruction. Thus, it depends on the M that we used to calibrate the data. We can also argue that we are using the BAO data and GP Pantheon+ reconstruction to determine the sound horizon, which we will use to predict BAO distances in a model-independent case. This might cause a preference for the reconstructed BAO distance ratios which can result in a high significance. This would be true if we take the predicted sound horizon for each measurement. However, we are considering the results of all of them, which weakens this effect. Our prediction of r_d is just adding a multiplicative factor to the predicted BAO distance ratios and not a redshift-dependent multiplicative factor that also changes the shape of the distance ratio-redshift evolution. Even so, we will make a test which will be independent of the value of r_d. This will be similar to the difference test that we made with the strong lensing results.

Furthermore, we can compare our determination of the sound horizon with the one from Planck 2018 assuming ΛCDM. This result is $r_d = 147.09 \pm 0.26$ Mpc [2]. The significance between of our determination $r_d = 135.09 \pm 3.47$ Mpc and this result of Planck is 0.056% (3.45σ). The relative difference is 8.8%. This tension accounts for a part of the 5σ tension between the H_0 result of SH0ES 2022 [1]

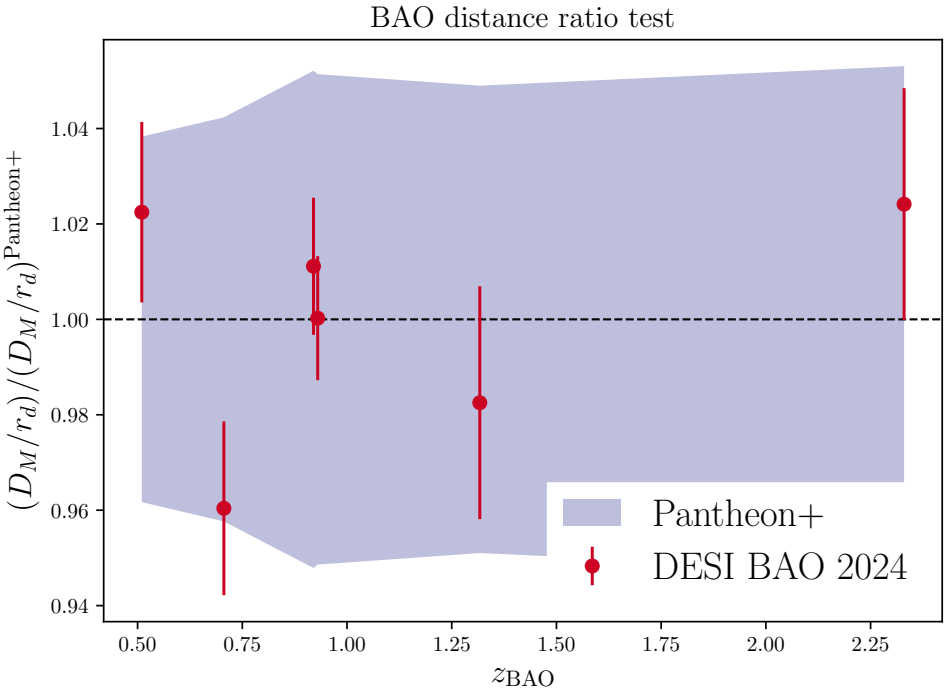

Figure 4.2: Comparison of the DESI BAO 2024 distance ratios D_M/r_d with the calibrated Pantheon+ reconstructed GP values $(D_M/r_d)_{\text{Pantheon+}}$.

and Planck 2018 [2]. Now, after predicting the value of the sound horizon, we are ready to reconstruct BAO distance ratios.

4.2 GP Reconstruction of the BAO Distance Ratios

Starting from the reconstructed Pantheon+ GP catalogue, we can derive the transverse comoving distances with

$$D_M(z) = \frac{1}{1+z}\, 10^{(\mu(z)+5)/5}\,\text{pc}. \tag{4.3}$$

The general method is to produce a large amount of samples, of the order of 10^5. We then compute the mean value and standard deviation. However, since we will deal with BAO distance ratios, we first need to divide the reconstructed

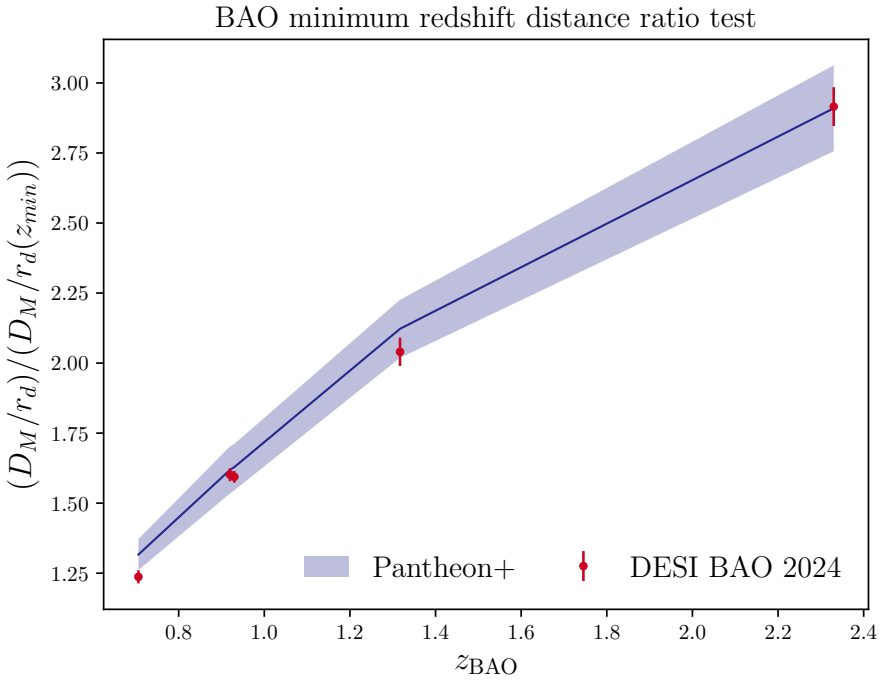

Figure 4.3: Comparison of the DESI BAO 2024 distance ratio $(D_M/r_d)/(D_M/r_d(z_{\rm min}))$ with the calibrated Pantheon+ reconstructed GP ratios $((D_M/r_d)/(D_M/r_d(z_{\rm min})))_{\rm Pantheon+}$.

transverse comoving distances by the samples of the sound horizon

$$\left(\frac{D_M(z)}{r_d}\right)_{\rm samples} = \frac{D_{M\ \rm samples}^{\rm Pantheon+}(z)}{r_{d\ \rm samples}}, \tag{4.4}$$

where we divide the samples to get the distance ratio samples. Since the number of samples is large, the result will be very close to a Gaussian one. Thus, after taking the ratio, we can compute the mean value and uncertainty. This will give us the GP reconstruction of the BAO distance ratio starting from the Pantheon+ catalogue. Let us recall that for the strong lensing reconstruction, we took the base 10 logarithms of the H0LiCOW data and the GP determination of the lensing distances. However, for the BAO distance ratios, we do not need to do this. This is because the measured BAO ratios are already Gaussian. Thus, we do not need to take the logarithm to get a better approximation of a Gaussian.

We present the predicted values for the Pantheon+ GP BAO ratios in table 4.2. We also included the measured values from DESI 2024 [14, 15] for comparison. As we can see, all the predicted values are consistent with the measured ones.

Tracer	z_{eff}	D_M/r_d	$(D_M/r_d)_{\text{Pantheon+}}$
LRG1	0.51	13.62 ± 0.25	13.32 ± 0.51
LRG2	0.71	16.85 ± 0.32	17.54 ± 0.74
LRG3	0.92	21.81 ± 0.31	21.6 ± 1.1
LRG3+LRG1	0.93	21.71 ± 0.28	21.7 ± 1.1
ELG2	1.32	27.79 ± 0.69	28.3 ± 1.4
Lyman-α	2.33	39.71 ± 0.95	38.8 ± 2.1

Table 4.2: Comparison of the measured DESI BAO ratios D_M/r_d and the predicted Pantheon+ BAO ratios $(D_M/r_d)_{\text{Pantheon+}}$. We include the uncertainties at 1σ C.L.

Furthermore, we can see that the uncertainties of the predicted BAO ratios are considerably higher. The reason for this is that to predict them, we took the ratio of two Gaussian quantities. We show the ratio of the measured quantities with respect to the reconstructed ratios from Pantheon+ in figure 4.2. Here, we can confirm that the reconstructed ratios are perfectly consistent with the measured ones. The significance (and C.L.) for the comparison of BAO distance ratios is 95.9% (0.0515σ). Thus, we validate that the agreement is way lower than 1σ. This means that if the reconstructed ratios were real data, they would not be in tension from DESI 2024.

We now turn our attention to the shape of the reconstructed curve. For this, we do the amplitude test with equation (3.17). The average amplitude of the DESI BAO 2024 distance ratios is $\langle D_M/r_d \rangle = 23.58 \pm 0.22$. On the other hand, for the reconstructed GP data from Pantheon+, we have $\langle (D_M/r_d)_{\text{Pantheon+}} \rangle = 23.53 \pm 0.64$. The significance between these results is 94.3% (0.072σ). This shows that the curve shape of the predicted distance ratios from Pantheon+ is fully consistent with the measured ones. We were talking about how building the r_d constraints from the predicted D_M Pantheon+ and the measured D_M/r_d could introduce a bias to the predicted values. However, we used the overall constraint r_d which only effectively adds a multiplicative factor to the predicted values from Pantheon+. Thus, by doing this, we are not changing the shape of the curve. Thus, this amplitude test is independent of the value that we took for the sound horizon r_d. We will examine this by performing a sound horizon r_d independent test.

For the strong lensing case, we performed a difference test. For this, we took the difference in the logarithm of the data with respect to the datum with

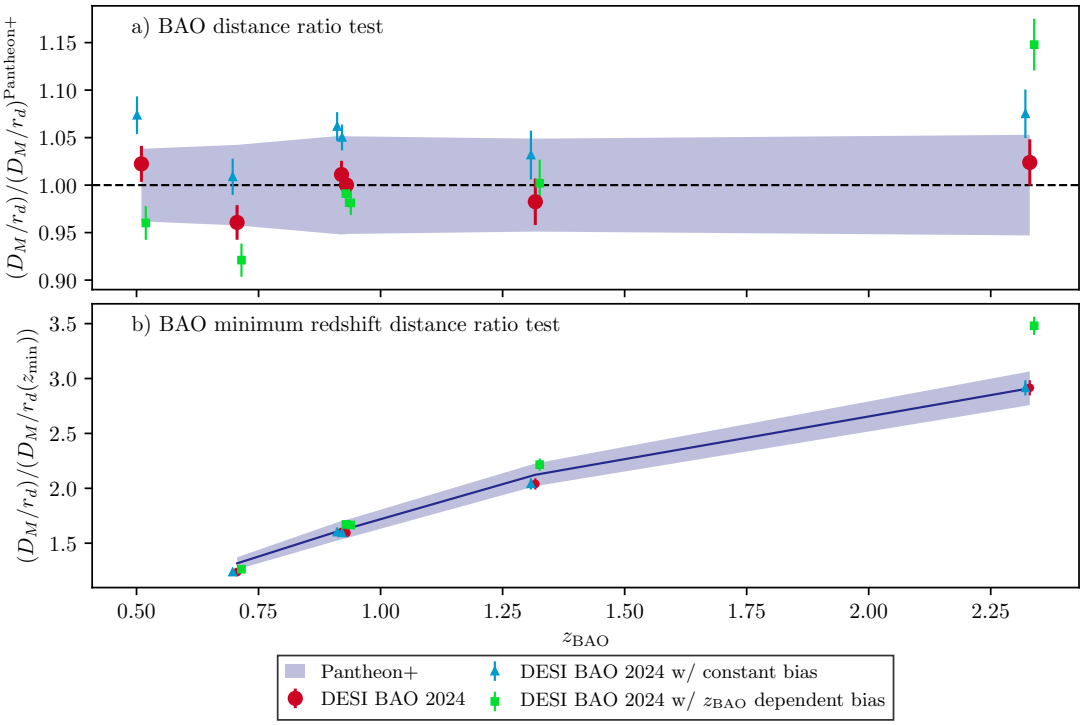

Figure 4.4: Comparison of the biased DESI BAO data with the GP reconstructed Pantheon+ data. This figure is similar to 4.2 and 4.3 but we are introducing a 5% constant bias to the BAO distance ratios D_M/r_d. Furthermore, we also include the results by introducing a redshift-dependent bias parametrized by $0.1(z_{\text{BAO}} - z_{\text{mean}})$ where z_{BAO} is the redshift of each measurement and z_{mean} the mean value of the redshifts of all measurements in the DESI BAO catalogue.

a lower redshift. We will repeat this analysis. The caveat is that we will consider the ratio instead of the difference. This is because we derive the DESI BAO 2024 measurements and not their logarithms. In this case, we are taking the ratio of the data (both the DESI BAO 2024 measurements and the reconstructed ones with Pantheon+) with the datum of small redshift. Thus, we are considering $(D_M/r_d(z))/(D_M/r_d(z_{\min}))$. The minimum corresponds to the BAO measurement with the LRG1 tracer. Since the sound horizon r_d is constant after recombination, this result is independent of this calibrator. Thus, this test will be completely independent of the value of the sound horizon. We know the mean values and covariance matrices for the data. To derive the mean values of this ratio with respect to minimum redshift we simply need to take the ratio of mean

values. On the other hand, the covariance of the ratio is given by

$$\Sigma_{i+1,j+1} \approx \frac{C_{i+1,j+1}}{\mu_1^2} + \frac{\mu_{i+1}\mu_{j+1}}{\mu_1^4} C_{1,1} - \frac{\mu_{i+1}}{\mu_1^3} C_{1,j+1} - \frac{\mu_{j+1}}{\mu_1^3} C_{1,i+1}, \tag{4.5}$$

where Σ is the covariance matrix of the ratio, C the covariance of the data, μ_1 is the mean value of the datum with the minimum redshift and the indexes $i+1$ and $j+1$ go over the data except the first element. We present the results of this analysis in figure 4.3. As we can see all the DESI BAO 2024 measurements are consistent with the Pantheon+ reconstruction at 1σ C.L., except the one at $z_{\rm BAO} = 0.706$. The significance of this comparison is 81% (0.241σ), which is way lower than 1σ C.L. This is a r_d-independent test and still confirms that the predicted reconstruction from Pantheon+ is fully consistent with the DESI data. We now turn our attention to the study of how these results change if we bias the DESI BAO data.

We start by introducing a +5% constant shift to the distance ratios D_M/r_d. This has a big impact on the significance, which is now 51.7% (0.648σ), considerably lower than the 95.9% significance for the unbiased data. The amplitude test gives $\langle D_M/r_d \rangle = 24.76 \pm 0.23$, having a significance of 7.03% (1.81σ) with the reconstructed data from Pantheon+. As we can see this bias severely impacts the agreement of the DESI BAO data with the reconstructed Pantheon+. Even so, the agreement is still under the 2σ C.L. It is useful to notice that causing a constant bias to the observed data is technically equivalent to changing the calibration of the sound horizon r_d. Thus, this shows that the level of agreement of the DESI BAO data and Pantheon+ is highly dependent on the calibration of the sound horizon r_d. Even so, the test where we compare the ratio of the data with the datum with the lowest redshift (the minimum redshift distance ratio test) is invariant under this bias. This is because the bias is redshift-independent. We can confirm this by computing the significance, which is 81.5% (0.233σ). This result is the same as the no-bias case (except for a sub-percent change).

Let us now study what happens when we consider a redshift-dependent bias parametrized by $0.1(z_{\rm BAO} - z_{\rm mean})$ with $z_{\rm BAO}$ the redshift of each BAO measurement and $z_{\rm mean}$ the mean values of all the redshift measurements. This bias causes a bigger shift in the agreement, having a significance of 9.1% (1.69σ), which is much lower than 95.9% for the unbiased data case. For the amplitude test, we

get $\langle D_M/r_d \rangle = 24.08 \pm 0.23$ having a significance of 42.2% (0.804σ). It is interesting how this result is higher than the case for +5% constant bias. Finally, the minimum redshift distance ratio test gives a significance of 2.89% (2.18σ). This breaks the 2σ threshold causing the reconstructed Pantheon+ data to be in tension with this redshift-dependent biased DESI data.

We plot the results of the bias tests in figure 4.4. As we can see, the constant bias data suffers changes that make the significance of the distance ratio test lower. However, for the minimum distance ratio test, the data is unchanged, as expected. For the redshift-dependent case, we see that the level of disagreement peaks for the datum with the highest redshift. This datum causes most of the decreased significance between the biased data and the reconstructed Pantheon+ data.

We summarize the analyses and findings now. They provide another model-independent consistency check between BAO distance ratio D_M/r_d data from DESI [14, 15] and SNeIa data from the Pantheon+ catalogue [13]. We used the GP Pantheon+ catalogue from the previous chapter to predict BAO distance ratios D_M/r_d and to compare them with the observational data from DESI BAO 2024. We started from the predicted GP distance modulus and computed the transverse comoving distances D_M. After this, we needed to derive the sound horizon r_d. We generated 10^5 Gaussian samples from the DESI BAO 2024 data D_M/r_s and from the GP reconstructed Pantheon+ catalogue D_M. By taking the ratio of the latter with the former, we got Gaussian samples for the sound horizon r_d. This effectively introduces a bias to our predicted BAO distance ratios. The cause of this is that we used the real BAO data to calibrate the sound horizon r_d and we used this result to predict the BAO distance ratios. That is why we took the r_d general constraint for all the data and not for any single redshift. Thus, by taking the ratio $D_M^{\text{Pantheon+}}$ to $r_d^{\text{constrained}}$ we are effectively dividing the predicted data by a constant and not a factor that changes the shape of the data and thus the predictions. This is because the sound horizon r_d is constant after recombination.

We compared the predicted distance ratios D_M/r_d of the DESI BAO 2024 with the GP reconstruction of Pantheon+ (distance ratio test) and found that their consistent with more than 90% significance. After this, we performed a

sound horizon-independent test. We divided both catalogues by the datum with minimum redshift (minimum redshift distance ratio test). We found an excellent agreement once again showing a significance higher than 80%. This confirms that the predicted data is fully consistent with the actual data. We also computed the overall amplitude and found excellent agreement as well.

We proceeded by including a bias to the DESI BAO 2024 data to see how the agreements change with this. We considered a +5% constant bias for the BAO distance ratios. We found that this bias causes disagreement between the biased data and the predicted data by turning the significance just over 50% (still under 1σ C.L.). However, the minimum redshift distance ratio showed the same significance except for sub-percent changes. This is expected since we biased all the BAO data by the same amount. We also considered a redshift-dependent bias parametrized by $0.1(z_{\rm BAO} - z_{\rm mean})$. This bias caused a bigger disagreement than the constant one, having a significance under 10%. The minimum redshift distance ratio showed even more disagreement with a significance of less than 3% which is more than 2σ C.L. Thus, the BAO DESI 2024 data would not be consistent with the Pantheon+ GP reconstruction if it is biased. Furthermore, we should notice that for this comparison, we took smaller biases of +5% for the constant case in comparison to +8% and +15% for the strong lensing case. On the other hand, we considered a redshift-dependent bias given by $0.1(z_{\rm BAO} - z_{\rm mean})$ in comparison to the $0.5(z_{\rm H0LiCOW} - z_{\rm mean})$ for the strong lensing catalogue. This shows how the consistency of the Pantheon+ GP reconstruction and DESI BAO 2024 are heavily dependent on biased data. If either catalogue has important unaccounted systematics or unaccounted biases, they would be in tension. Even so, the tension would not be close to the 5σ C.L. that SH0ES 2022 and Planck 2018 currently have. In addition to this, as we can see from the constant bias test, a miscalibration of the sound horizon r_d would produce a tension between the predicted BAO ratios and the measured ones. However, this would not affect the minimum redshift distance ratio test since it is fully independent of the value of the sound horizon r_d.

In this chapter, we showed that by starting from the SNeIa Pantheon+ catalogue [13], we can predict the distance ratios of DESI BAO 2022 [14, 15] and they are perfectly compatible. This is the second test of this nature presented in this thesis after the first one comparing the predicted Pantheon+ lensing distances

to the ones from the H0LiCOW collaboration [12]. These tests are completely model-independent and thus are not biased towards a particular Cosmological model. However, one of the tests performed in this chapter introduced a bias that might cause a better agreement between the predicted Pantheon+ GP distance ratios and the actual data from DESI BAO. For this, we computed the sound horizon r_d assuming the full BAO dataset and the SNeIa prediction for the transverse comoving distance. Even so, we argue that we are considering the overall constraints and not a redshift-dependent constraint that would change the shape of the predicted distance ratios. This would increase the bias and the agreement even more. Despite this, we did a second test which is independent of the sound horizon r_d calibration. This gives further support that the predictions are consistent with the actual data. Since the test is model-independent, we have further evidence that there are no unaccounted systematic effects on both datasets (Pantheon+ and DESI BAO). This implies that we present more evidence for the hypothesis that we require a new standard model of Cosmology different to ΛCDM to solve the H_0 between SH0ES 2022 [1] and Planck 2018 [2].

All our tests presented in this chapter showed an agreement way lower than 1σ C.L. for both r_d-dependent and r_d-independent tests. As we said in the previous chapter, there was still the possibility that both H0LiCOW and Pantheon+ are subject to the systematics of the same sign, magnitude and redshift dependence [10]. Thus, from the consistency tests that we performed in the last chapter, we could not discard this possibility. Even so, this scenario is highly unlikely. The analysis presented in this chapter reduces even more the probability of this unlikely possibility. We saw that Pantheon+ predictions are compatible with both strong lensing measurements and BAO distance ratios. The only assumptions that we made to build this reconstructed data were that the value of the Hubble constant from SH0ES 2022 [1] is accurate and that the Universe is flat. Thus, these tests also support the premise that the cosmic distance ladder method is not affected by unknown systematics. Even more, this test with BAO and Pantheon+ gives less freedom for unknown systematics. As we saw, even a small bias of around 5% to the BAO distance ratio creates a disagreement of almost 2σ C.L. with the Pantheon+ predictions. This was not seen with H0LiCOW and Pantheon+ even by considering 10% and 15% biases. This bias can come from a wrong determination of the sound horizon r_d. For instance, the difference between our calibration of r_d and the one for Planck 2018 is 8.8%. Thus, a calibration

of the data with the Planck sound horizon r_d would cause tension between BAO and Pantheon+ predictions. Furthermore, the tests are very sensible of redshift-dependent biases. A $0.1(z_{\rm BAO} - z_{\rm mean})$ causes a 2σ C.L. tension. All of these facts show the importance of comparing BAO distance ratios and Pantheon+ predictions.

Conclusions

In this thesis, we performed two distance-redshift consistency tests from Type 1a Supernova (SNeIa) and two observables: strong lensing measurements and Baryon Acoustic Oscillation (BAO) distance ratios. We uploaded the results from [10] by using the update of the Pantheon catalogue [11], Pantheon+ [13]. Furthermore, we used the last result of H_0 from the SH0ES collaboration [1] to calibrate the SNeIa data.

Our tests started by generating a continuous version of the Pantheon+ catalogue. We did it with a Gaussian process (GP) regression interpolation. We checked that our continuous reconstruction was consistent with Pantheon+ by performing three tests. We checked that the distance modulus residuals were consistent with the ones from the binned Pantheon+ catalogue. We found a good agreement with almost all measurements from the Pantheon+ catalogue close to the mean value of the GP reconstructions. For the remaining measurements, they were always consistent with the GP at the 1σ C.L. Then, we plotted the covariance matrix of the binned Pantheon+ catalogue and the reconstruction using the GP and found that they were very similar in the diagonal and just showed slight differences in the non-diagonal elements. Finally, we performed a Monte Carlo Markov Chain method to fit the GP reconstruction data as if it were real data and compare it with the constraints of the full Pantheon+ catalogue. For this part, we assumed the ΛCDM model but the reconstructed data is model independent. We found that the confidence regions were almost identical with minimal differences. Thus, these consistency tests show that our reconstructed continuous version of the Pantheon+ is accurate.

We proceeded to predict the strong lensing distances and BAO distance ratios from this GP reconstruction. This catalogue gives us a prediction for the distance modulus $\mu(z) = m(z) - M$ for any redshift once we calibrate the absolute mag-

nitude M. From them, we can derive the predicted luminosity distance at any redshift. This allows us to predict the strong lensing data. We start with the lens distance which is an angular distance. Then, we focus on the time delay distance given as products of redshift and angular diameter distances. For the BAO distance ratios, we need to compute D_M/r_d which is the ratio of the transverse moving distance to the sound horizon. After this, we compared the actual data with the predictions from the GP reconstruction using the Pantheon+ catalogue. This was to test the agreement and to study whether the cosmic distance ladder determination of the Hubble constant H_0 can be subject to unknown systematic errors. We then created two sets of simulated data. We did this by introducing a constant bias and a redshift-dependent bias to the actual data. Then, we study how the level of agreement changed and if the biases could introduce statistical tensions.

Since the strong Lensing data from the H0LiCOW collaboration [12] was not Gaussian, we took the base 10 logarithm of the data which was almost perfectly Gaussian. This was to make an accurate comparison to the Gaussian predicted data. The first test consisted of computing the ratio of the actual data to the predicted one from Pantheon+ and taking the base 10 logarithm. This is called the distance ratio test. We found a perfect agreement which was way lower than the 1σ C.L. For the second test, we performed the amplitude test, which is an average value of the base 10 logarithm of the distances. We also found a perfect agreement better than the previous test and also way below the 1σ C.L. For the third test, we divided the actual data and predicted data by the datum with the smallest lens redshift. This test is H_0-independent. We call it the minimum redshift test. We compared the results of the actual data and predicted data to test the agreement. Once again, the results proved that the agreement is good, way below the 1σ C.L. After this, we introduced a bias to the actual data from H0LiCOW. We considered a constant bias with 10% for the time delay distances $D_{\Delta t}$ and 15% for the lensing distances D_l. This introduced some disagreement but it was always under 2σ C.L. This shows that even with considerable percentage constant biases, the comparison is still statistically consistent. We finally considered a redshift-dependent bias parametrized by $0.5(z_{\rm lens} - \text{mean})$. This bias had a tension over 2σ C.L. between the actual and predicted values. This indicates that a redshift-dependent bias could produce tension in our results. Thus, the comparison does not allow big redshift-dependent biases.

The BAO measurements from the DESI collaboration [14, 15] offer constraints on D_M/r_d, the ratio of the transverse comoving distance to the sound horizon. We derived D_M from the predictions of the continuous Pantheon+ catalogue. However, for the sound horizon, we needed to derive an additional constraint. We took all the BAO measurements and generated Gaussian samples which we called $(D_M/r_d)_{\text{samples}}$. Then, we generated samples from the derived predictions $(D_M)^{\text{Pantheon+}}_{\text{samples}}$ of Pantheon+. We finally got the sound horizon r_d samples with $r_{d\,\text{samples}} = ((D_M/r_d)_{\text{samples}})/(D_M)^{\text{Pantheon+}}_{\text{samples}}$. We considered the full BAO catalogue to avoid introducing severe biases to our results. We took the mean value and variance of the samples to derive the mean and standard deviation. We generated the predicted samples by taking the ratio $D_M^{\text{Pantheon+}}/r_d$. Notice that our samples are dependent on a calibration of the sound horizon. However, since it is constant after recombination, it is a multiplicative factor that does not change the shape of the predicted data. For the BAO distance ratio test, which consists of comparing the DESI BAO 2024 data [14, 15] to the predicted data from Pantheon+, we got a perfect agreement showing more than 90% significance and agreement way lower 1σ C.L. We also implemented a sound horizon-independent test. We divided both catalogues by the datum with the minimum redshift. This is called the minimum redshift ratio test. After comparing the results from both datasets, we found an excellent agreement with significance over 80%. Once again, this is way lower than 1σ C.L. The overall amplitude showed excellent agreement as well. We included biases similar to the case of strong lensing. We started with a +5% constant bias for the actual BAO distance ratios. This bias caused a discrepancy between the observational BAO and predicted data, lowering the significance by just over 50%. However, this is still under 1σ C.L. The minimum redshift distance ratio test showed the same results as the unbiased data except for sub-percent changes. This is expected since we are biasing the data by the same amount and not in a redshift-dependent way. We should notice that introducing a constant bias to the data is equivalent to changing the calibration of the sound horizon r_d. Thus, this shows that the level of agreement between the actual and predicted data is highly dependent on the calibration of r_d. If we took the result from Planck 2018 [2] assuming ΛCDM, we would get a tension between DESI BAO 2022 and the Pantheon+ predictions. However, this would not be measured in the minimum redshift distance ratio test since it is sound horizon-independent. This gives us an interesting idea for future research.

We could compute the range of acceptable values that the sound horizon r_d can get for the Pantheon+ predictions to be consistent with BAO data. This can be further extended to more BAO and SNeIa catalogues.

For the comparison between BAO and the Pantheon+ distance ratios predictions, we considered a redshift-dependent bias as well. This is parametrized by $0.1(z_{\rm BAO} - z_{\rm mean})$. This is 80% smaller than the bias for the strong lensing case of $0.5(z_{\rm H0LiCOW} - z_{\rm mean})$. This bias caused a huge disagreement between the data and the predicted values. It had a significance of just over 9%, which is still under 2σ C.L. for the BAO distance ratio test. However, for the minimum redshift distance ratio test, there is a significance of just over 2%, which is in tension with the predicted values from Pantheon+ at over 2σ C.L. This tension shows that the BAO data cannot have big unaccounted systematic errors to allow a good agreement. Even so, the tension is still way lower than the 5σ C.L. tension between the H_0 value of SH0ES 2022 and Planck 2018.

As we can see, in this thesis we showed that we can predict strong lens distances and BAO distance ratios starting from SNeIa data. We need to assume a calibration of the absolute magnitude M that allows SNeIa to work as standard candles. We took the calibration from the last result of the SH0ES collaboration [1]. We did it to perform consistency tests and to find out if the analysis conducted by the SH0ES collaboration in determining H_0 is subject to unknown systematic errors. Our other assumption was that the Universe is spatially flat. This is a reasonable assumption because the CMB points to a Universe with no curvature. Furthermore, inflation washes out any initial curvature that the Universe could have. We predicted the observational values of strong lensing and BAO distance ratios and found that they were perfectly compatible. These tests were done in a model-independent way. Thus, the level of agreement suggests that there are no unaccounted systematics on Pantheon+, DESI BAO and H0LiCOW. This also implies that we need a new standard model of Cosmology different to the current one, ΛCDM. This new model should solve the H_0 tension between SH0ES 2022 and Planck 2018. We got even more evidence of all of this by considering biases of the data that could be produced from unaccounted systematic errors. We found that wrong determinations of the Hubble constant H_0 or the sound horizon r_d would cause disagreements between the observational data and the predicted one using Pantheon+. As a strong example, we can remember that we considered a

+5% constant bias in the BAO observations. This gave a level of disagreement of almost 2σ C.L. between Pantheon+ and DESI BAO 2024. For comparison, the difference between our calibration of r_d and the result from Planck 2018 is 8.8%. Thus, if we calibrated our data with the sound horizon from Planck, we would get a tension between the BAO data and our GP predictions. In addition to this, we showed that the level of agreement is very sensible of redshift-dependent biases. When considering them, we had tensions of more than 2σ C.L. All of these results provide strong evidence that there are no unaccounted systematic errors in the Hubble constant H_0 measurement of the SH0ES collaboration. Thus the problem needs to be solved by new physics beyond ΛCDM. The results obtained in this thesis will be published in an international journal.

The analyses of this thesis can be repeated using other SNeIa catalogues to test the level of agreement that they have with strong lensing and BAO catalogues. Furthermore, it is possible to extend it to other BAO samples. In addition to this, we can revisit the Gaussian Process (GP) reconstruction to predict the derivative of the Luminosity distance with redshift. This would enable a prediction on the Hubble parameter at different redshifts. Thus, we would be able to compare these results with the D_H/r_d distance ratios from the DESI BAO data where $D_H = c/H(z)$ is the Hubble distance. Moreover, this would enable a different way to calibrate the sound horizon similar to the method that we used with transverse comoving distances. Finally, it would be possible to predict the value of the ratio D_M/D_H which is also reported by the DESI collaboration. This would make it possible to make further studies with sound horizon-independent measurements. Finally, it is also possible to start from the BAO data and perform different calibrations on the sound horizon r_d for the predicted data using Pantheon+. We can then compute the significances using the distance ratio tests to determine the possible values that the sound horizon can have to have a consistency between the predicted Pantheon+ measurements and the actual BAO measurements. These tests would provide stronger evidence for our conclusions.

As we saw, our results support the claim that the distance ladder determination of H_0 using Cepheids and SNeIa is not under the influence of unknown systematic errors. This in turn implies that the Cosmological crisis of the Hubble constant tension problem H_0 seems to have a physical origin. Thus, to solve this problem, among others that Cosmology is having nowadays, we need to propose

alternative models to ΛCDM in the form of dynamic dark energy, scalar field dark energy, new particles in the particle standard model, modified and extended theories of gravity or more possibilities.

References

[1] Adam G Riess et al. “A comprehensive measurement of the local value of the Hubble constant with 1 km s- 1 Mpc- 1 uncertainty from the Hubble Space Telescope and the SH0ES team”. In: *The Astrophysical journal letters* 934.1 (2022), p. L7 (cit. on pp. 1, 3, 11, 15, 17, 21, 22, 37–39, 41, 42, 44, 48, 50, 52, 56, 59, 67, 69, 72).

[2] Nabila Aghanim et al. “Planck 2018 results-VI. Cosmological parameters”. In: *Astronomy & Astrophysics* 641 (2020), A6 (cit. on pp. 1, 11, 13, 21, 22, 37, 40, 44, 56, 59, 60, 67, 71).

[3] Eleonora Di Valentino et al. “In the realm of the Hubble tension—a review of solutions”. In: *Classical and Quantum Gravity* 38.15 (2021), p. 153001 (cit. on p. 1).

[4] Licia Verde, Nils Schöneberg, and Héctor Gil-Marín. “A tale of many H 0”. In: *Annual Review of Astronomy and Astrophysics* 62 (2023) (cit. on p. 1).

[5] T Shanks et al. “Local Hole revisited: evidence for bulk motions and self-consistent outflow”. In: *Monthly Notices of the Royal Astronomical Society* 490.4 (2019), pp. 4715–4720 (cit. on pp. 1, 22).

[6] Lloyd Knox and Marius Millea. “Hubble constant hunter’s guide”. In: *Physical Review D* 101.4 (2020), p. 043533 (cit. on pp. 1, 18–20).

[7] Silvia Masi et al. “The BOOMERanG experiment and the curvature of the universe”. In: *Progress in Particle and Nuclear Physics* 48.1 (2002), pp. 243–261 (cit. on p. 1).

[8] Tilman Tröster et al. “Cosmology from large-scale structure-Constraining ΛCDM with BOSS”. In: *Astronomy & Astrophysics* 633 (2020), p. L10 (cit. on p. 1).

[9] Adam G Riess et al. “Observational evidence from supernovae for an accelerating universe and a cosmological constant”. In: *The astronomical journal* 116.3 (1998), p. 1009 (cit. on pp. 1, 26).

[10] Shivam Pandey, Marco Raveri, and Bhuvnesh Jain. "Model independent comparison of supernova and strong lensing cosmography: Implications for the Hubble constant tension". In: *Physical Review D* 102.2 (2020), p. 023505 (cit. on pp. 2, 3, 22, 37, 40–43, 45, 47, 48, 52–54, 56, 67, 69).

[11] Daniel Moshe Scolnic et al. "The complete light-curve sample of spectroscopically confirmed SNe Ia from Pan-STARRS1 and cosmological constraints from the combined pantheon sample". In: *The Astrophysical Journal* 859.2 (2018), p. 101 (cit. on pp. 2, 22, 27, 37, 69).

[12] Kenneth C Wong et al. "H0LiCOW–XIII. A 2.4 per cent measurement of H 0 from lensed quasars: 5.3 σ tension between early-and late-Universe probes". In: *Monthly Notices of the Royal Astronomical Society* 498.1 (2020), pp. 1420–1439 (cit. on pp. 2, 22, 38, 39, 44, 54, 57, 67, 70).

[13] Dan Scolnic et al. "The Pantheon+ analysis: the full data set and light-curve release". In: *The Astrophysical Journal* 938.2 (2022), p. 113 (cit. on pp. 2, 22, 28, 29, 37, 38, 41, 50, 54, 65, 66, 69).

[14] AG Adame et al. "DESI 2024 III: Baryon Acoustic Oscillations from Galaxies and Quasars". In: *arXiv preprint arXiv:2404.03000* (2024) (cit. on pp. 2, 22, 34, 35, 59, 61, 65, 66, 71).

[15] AG Adame et al. "DESI 2024 IV: Baryon Acoustic Oscillations from the Lyman Alpha Forest". In: *arXiv preprint arXiv:2404.03001* (2024) (cit. on pp. 2, 22, 34, 35, 59, 61, 65, 66, 71).

[16] Lucas Lombriser. "Consistency of the local Hubble constant with the cosmic microwave background". In: *Physics Letters B* 803 (2020), p. 135303 (cit. on p. 3).

[17] S Taubenberger et al. "The Hubble constant determined through an inverse distance ladder including quasar time delays and Type Ia supernovae". In: *Astronomy & Astrophysics* 628 (2019), p. L7 (cit. on p. 3).

[18] Nikki Arendse et al. "Cosmic dissonance: are new physics or systematics behind a short sound horizon?" In: *Astronomy & Astrophysics* 639 (2020), A57 (cit. on p. 3).

[19] Kai Liao et al. "A model-independent determination of the Hubble constant from lensed quasars and supernovae using Gaussian process regression". In: *The Astrophysical Journal Letters* 886.1 (2019), p. L23 (cit. on p. 3).

[20] Kai Liao et al. “Determining model-independent H0 and consistency tests”. In: *The Astrophysical Journal Letters* 895.2 (2020), p. L29 (cit. on p. 3).

[21] CS Kochanek. “Overconstrained gravitational lens models and the Hubble constant”. In: *Monthly Notices of the Royal Astronomical Society* 493.2 (2020), pp. 1725–1735 (cit. on p. 3).

[22] M Rigault et al. “Confirmation of a star formation bias in type Ia supernova distances and its effect on the measurement of the Hubble constant”. In: *The Astrophysical Journal* 802.1 (2015), p. 20 (cit. on p. 3).

[23] M Rigault et al. “Strong dependence of Type Ia supernova standardization on the local specific star formation rate”. In: *Astronomy & Astrophysics* 644 (2020), A176 (cit. on p. 3).

[24] DO Jones et al. “Should Type Ia supernova distances be corrected for their local environments?” In: *The Astrophysical Journal* 867.2 (2018), p. 108 (cit. on p. 3).

[25] Peter Schneider and Dominique Sluse. “Source-position transformation: an approximate invariance in strong gravitational lensing”. In: *Astronomy & Astrophysics* 564 (2014), A103 (cit. on p. 3).

[26] Dandan Xu et al. “Lens galaxies in the Illustris simulation: power-law models and the bias of the Hubble constant from time delays”. In: *Monthly Notices of the Royal Astronomical Society* 456.1 (2016), pp. 739–755 (cit. on p. 3).

[27] Sandra Unruh, Peter Schneider, and Dominique Sluse. “Ambiguities in gravitational lens models: the density field from the source position transformation”. In: *Astronomy & Astrophysics* 601 (2017), A77 (cit. on p. 3).

[28] Alessandro Sonnenfeld. “On the choice of lens density profile in time delay cosmography”. In: *Monthly Notices of the Royal Astronomical Society* 474.4 (2018), pp. 4648–4659 (cit. on p. 3).

[29] Oliver Piattella et al. *Lecture notes in cosmology*. Tech. rep. Springer, 2018 (cit. on pp. 6, 30).

[30] Bernard Schutz. *A first course in general relativity*. Cambridge university press, 2022 (cit. on pp. 7, 8).

[31] Gary Hinshaw et al. “Nine-year Wilkinson Microwave Anisotropy Probe (WMAP) observations: cosmological parameter results”. In: *The Astrophysical Journal Supplement Series* 208.2 (2013), p. 19 (cit. on p. 13).

[32] Simone Aiola et al. “The Atacama Cosmology Telescope: DR4 maps and cosmological parameters”. In: *Journal of Cosmology and Astroparticle Physics* 2020.12 (2020), p. 047 (cit. on p. 13).

[33] David W Hogg. “Distance measures in cosmology”. In: *arXiv preprint astro-ph/9905116* (1999) (cit. on pp. 14, 15).

[34] Adam G Riess et al. “A redetermination of the Hubble constant with the Hubble Space Telescope from a differential distance ladder”. In: *The Astrophysical Journal* 699.1 (2009), p. 539 (cit. on pp. 16, 21).

[35] Sudipta Das. “Aspects of quintessence matter-the driver of the late time acceleration of the universe”. In: *arXiv preprint arXiv:0808.0826* (2008) (cit. on p. 17).

[36] Adam G Riess et al. “Cosmic distances calibrated to 1% precision with Gaia EDR3 parallaxes and Hubble Space Telescope photometry of 75 Milky Way Cepheids confirm tension with ΛCDM”. In: *The Astrophysical Journal Letters* 908.1 (2021), p. L6 (cit. on pp. 17, 21).

[37] Kayla A Owens et al. “Current challenges in Cepheid distance calibrations using Gaia early data release 3”. In: *The Astrophysical Journal* 927.1 (2022), p. 8 (cit. on p. 17).

[38] Lucas M Macri et al. “A new Cepheid distance to the maser-host galaxy NGC 4258 and its implications for the Hubble Constant”. In: *The Astrophysical Journal* 652.2 (2006), p. 1133 (cit. on p. 17).

[39] Georges Paturel et al. “Calibration of the distance scale from galactic Cepheids-I. Calibration based on the GFG sample”. In: *Astronomy & Astrophysics* 383.2 (2002), pp. 398–409 (cit. on p. 17).

[40] Dale J Fixsen et al. “The cosmic microwave background spectrum from the full cobe* firas data set”. In: *The Astrophysical Journal* 473.2 (1996), p. 576 (cit. on p. 18).

[41] Edward L Wright et al. “Interpretation of the COBE FIRAS CMBR spectrum”. In: *The Astrophysical Journal, Part 1 (ISSN 0004-637X), vol. 420, no. 2, p. 450-456* 420 (1994), pp. 450–456 (cit. on p. 18).

[42] Nabila Aghanim et al. “Planck intermediate results-LI. Features in the cosmic microwave background temperature power spectrum and shifts in cosmological parameters”. In: *Astronomy & Astrophysics* 607 (2017), A95 (cit. on pp. 19, 20).

[43] Jan Tauber et al. “Planck 2013 results. XVI. Cosmological parameters”. In: *Astronomy & Astrophysics* 571 (2014), A16–A82 (cit. on pp. 20, 21).

[44] Wayne Hu, Naoshi Sugiyama, and Joseph Silk. “The physics of microwave background anisotropies”. In: *Nature* 386.6620 (1997), pp. 37–43 (cit. on p. 20).

[45] Adam G Riess et al. “A 3% solution: determination of the Hubble constant with the Hubble Space Telescope and Wide Field Camera 3”. In: *The Astrophysical Journal* 730.2 (2011), p. 119 (cit. on p. 21).

[46] Adam G Riess et al. “A 2.4% determination of the local value of the Hubble constant”. In: *The Astrophysical Journal* 826.1 (2016), p. 56 (cit. on pp. 21, 48).

[47] Adam G Riess et al. “New parallaxes of galactic cepheids from spatially scanning the hubble space telescope: Implications for the hubble constant”. In: *The Astrophysical Journal* 855.2 (2018), p. 136 (cit. on p. 21).

[48] Adam G Riess et al. “Large Magellanic Cloud Cepheid standards provide a 1% foundation for the determination of the Hubble constant and stronger evidence for physics beyond ΛCDM”. In: *The Astrophysical Journal* 876.1 (2019), p. 85 (cit. on pp. 21, 37, 52).

[49] J Dunkley et al. “Five-year wilkinson microwave anisotropy probe* observations: likelihoods and parameters from the Wmap data”. In: *The Astrophysical Journal Supplement Series* 180.2 (2009), p. 306 (cit. on p. 21).

[50] Eiichiro Komatsu et al. “Five-year wilkinson microwave anisotropy probe* observations: cosmological interpretation”. In: *The Astrophysical Journal Supplement Series* 180.2 (2009), p. 330 (cit. on p. 21).

[51] Charles L Bennett et al. “Nine-year Wilkinson Microwave Anisotropy Probe (WMAP) observations: final maps and results”. In: *The Astrophysical Journal Supplement Series* 208.2 (2013), p. 20 (cit. on p. 21).

[52] Peter AR Ade et al. “Planck 2015 results-xiii. cosmological parameters”. In: *Astronomy & Astrophysics* 594 (2016), A13 (cit. on p. 21).

[53] Louise Breuval et al. “Small Magellanic Cloud Cepheids Observed with the Hubble Space Telescope Provide a New Anchor for the SH0ES Distance Ladder”. In: *arXiv preprint arXiv:2404.08038* (2024) (cit. on p. 22).

[54] Sherry H Suyu et al. “H0LiCOW–I. H 0 Lenses in COSMOGRAIL’s Wellspring: program overview”. In: *Monthly Notices of the Royal Astronomical Society* 468.3 (2017), pp. 2590–2604 (cit. on p. 22).

[55] David W Hogg, Jo Bovy, and Dustin Lang. “Data analysis recipes: Fitting a model to data”. In: *arXiv preprint arXiv:1008.4686* (2010) (cit. on p. 23).

[56] David JC MacKay. *Information theory, inference and learning algorithms*. Cambridge university press, 2003 (cit. on p. 24).

[57] Rudolph Minkowski. “Spectra of supernovae”. In: *A Source Book in Astronomy and Astrophysics, 1900–1975*. Harvard University Press, 1979, pp. 478–480 (cit. on p. 25).

[58] Gertrud Contardo. “Analysis of Light Curves of Type Ia Supernovae”. PhD thesis. Technische Universität München, 2001 (cit. on p. 25).

[59] Mario Hamuy et al. “The absolute luminosities of the Calan/Tololo type IA supernovae”. In: *arXiv preprint astro-ph/9609059* (1996) (cit. on pp. 25, 26).

[60] Mark M Phillips. “The absolute magnitudes of Type IA supernovae”. In: *Astrophysical Journal, Part 2-Letters (ISSN 0004-637X), vol. 413, no. 2, p. L105-L108.* 413 (1993), pp. L105–L108 (cit. on p. 26).

[61] Adam G Riess, William H Press, and Robert P Kirshner. “A precise distance indicator: Type Ia supernova multicolor light-curve shapes”. In: *The Astrophysical Journal* 473.1 (1996), p. 88 (cit. on p. 26).

[62] Robert Tripp. “A two-parameter luminosity correction for Type IA supernovae”. In: *Astronomy and Astrophysics, v. 331, p. 815-820 (1998)* 331 (1998), pp. 815–820 (cit. on p. 28).

[63] JP Hu et al. “Testing the cosmological principle with the Pantheon+ sample and the region-fitting method”. In: *Astronomy & Astrophysics* 681 (2024), A88 (cit. on p. 28).

[64] Ryan J Foley et al. “The Foundation Supernova Survey: motivation, design, implementation, and first data release”. In: *Monthly Notices of the Royal Astronomical Society* 475.1 (2018), pp. 193–219 (cit. on p. 28).

[65] Mohan Ganeshalingam et al. “Results of the Lick Observatory supernova search follow-up photometry program: BVRI light curves of 165 type Ia supernovae”. In: *The Astrophysical Journal Supplement Series* 190.2 (2010), p. 418 (cit. on p. 28).

[66] Benjamin E Stahl et al. “Lick Observatory Supernova Search follow-up program: photometry data release of 93 Type Ia supernovae”. In: *Monthly Notices of the Royal Astronomical Society* 490.3 (2019), pp. 3882–3907 (cit. on p. 28).

[67] Dillon Brout et al. “First cosmology results using Type Ia supernovae from the Dark Energy Survey: photometric pipeline and light-curve data release”. In: *The Astrophysical Journal* 874.1 (2019), p. 106 (cit. on p. 28).

[68] Hideo Kodama and Misao Sasaki. “Cosmological perturbation theory”. In: *Progress of Theoretical Physics Supplement* 78 (1984), pp. 1–166 (cit. on p. 29).

[69] James M Bardeen. “Gauge-invariant cosmological perturbations”. In: *Physical Review D* 22.8 (1980), p. 1882 (cit. on p. 29).

[70] Leandro Manuel Pardo Calderón. “Baryon Acoustic Oscillations. Equation and physical interpretation”. In: *Scientia et technica* 23.2 (2018), pp. 262–267 (cit. on pp. 30, 31).

[71] Alessandra Grassi. “Baryon acoustic oscillations and primordial non-Gaussianities with weak lensing”. PhD thesis. 2013 (cit. on pp. 30–32).

[72] J Lesgourges. “Cosmological perturbations”. In: *Searching for New Physics at Small and Large Scales: TASI 2012*. World Scientific, 2013, pp. 29–97 (cit. on p. 31).

[73] Eric V Linder. “Lensing time delays and cosmological complementarity”. In: *Physical Review D—Particles, Fields, Gravitation, and Cosmology* 84.12 (2011), p. 123529 (cit. on p. 39).

[74] Tommaso Treu and Philip J Marshall. “Time delay cosmography”. In: *The Astronomy and Astrophysics Review* 24 (2016), pp. 1–41 (cit. on p. 39).

[75] Dan Coe and Leonidas A Moustakas. “Cosmological constraints from gravitational lens time delays”. In: *The Astrophysical Journal* 706.1 (2009), p. 45 (cit. on p. 39).

[76] C Vanderriest et al. “The value of the time delay Delta t (A, B) for the’double’quasar 0957+ 561 from optical photometric monitoring”. In: *Astronomy and Astrophysics (ISSN 0004-6361), vol. 215, no. 1, May 1989, p. 1-13.* 215 (1989), pp. 1–13 (cit. on p. 39).

[77] CR Keeton and CS Kochanek. "Determining the Hubble constant from the gravitational lens PG 1115+ 080". In: *The Astrophysical Journal* 487.1 (1997), p. 42 (cit. on p. 39).

[78] Vivien Bonvin et al. "H0LiCOW–V. New COSMOGRAIL time delays of HE 0435- 1223: H 0 to 3.8 per cent precision from strong lensing in a flat ΛCDM model". In: *Monthly Notices of the Royal Astronomical Society* 465.4 (2017), pp. 4914–4930 (cit. on p. 39).

[79] Sjur Refsdal. "On the possibility of determining Hubble's parameter and the masses of galaxies from the gravitational lens effect". In: *Monthly Notices of the Royal Astronomical Society* 128.4 (1964), pp. 307–310 (cit. on p. 39).

[80] Sjur Refsdal and Jean Surdej. "Gravitational lenses". In: *Reports on Progress in Physics* 57.2 (1994), p. 117 (cit. on p. 39).

[81] SH Suyu et al. "Dissecting the gravitational lens B1608+ 656. II. Precision measurements of the Hubble constant, spatial curvature, and the dark energy equation of state". In: *The Astrophysical Journal* 711.1 (2010), p. 201 (cit. on pp. 39, 40).

[82] Inh Jee et al. "A measurement of the Hubble constant from angular diameter distances to two gravitational lenses". In: *Science* 365.6458 (2019), pp. 1134–1138 (cit. on p. 40).

[83] Sherry H Suyu et al. "Cosmology from gravitational lens time delays and Planck data". In: *The Astrophysical Journal Letters* 788.2 (2014), p. L35 (cit. on p. 40).

[84] Geoff CF Chen et al. "A SHARP view of H0LiCOW: H 0 from three time-delay gravitational lens systems with adaptive optics imaging". In: *Monthly Notices of the Royal Astronomical Society* 490.2 (2019), pp. 1743–1773 (cit. on p. 40).

[85] Kenneth C Wong et al. "H0LiCOW–IV. Lens mass model of HE 0435-1223 and blind measurement of its time-delay distance for cosmology". In: *Monthly Notices of the Royal Astronomical Society* 465.4 (2017), pp. 4895–4913 (cit. on p. 40).

[86] S Birrer et al. "H0LiCOW–IX. Cosmographic analysis of the doubly imaged quasar SDSS 1206+ 4332 and a new measurement of the Hubble constant". In: *Monthly Notices of the Royal Astronomical Society* 484.4 (2019), pp. 4726–4753 (cit. on p. 40).

[87] Cristian E Rusu et al. “H0LiCOW XII. Lens mass model of WFI2033- 4723 and blind measurement of its time-delay distance and H 0”. In: *Monthly Notices of the Royal Astronomical Society* 498.1 (2020), pp. 1440–1468 (cit. on p. 40).

[88] Richard Kessler et al. “SNANA: A public software package for supernova analysis”. In: *Publications of the Astronomical Society of the Pacific* 121.883 (2009), p. 1028 (cit. on p. 41).

[89] J Buchner et al. “X-ray spectral modelling of the AGN obscuring region in the CDFS: Bayesian model selection and catalogue”. In: *Astronomy & Astrophysics* 564 (2014), A125 (cit. on p. 42).

[90] Matthias Seeger. “Gaussian processes for machine learning”. In: *International journal of neural systems* 14.02 (2004), pp. 69–106 (cit. on pp. 45, 47).

[91] Solomon Kullback and Richard A Leibler. “On information and sufficiency”. In: *The annals of mathematical statistics* 22.1 (1951), pp. 79–86 (cit. on p. 47).

[92] Kevin Aylor et al. “Sounds discordant: Classical distance ladder and ΛCDM-based determinations of the cosmological sound horizon”. In: *The Astrophysical Journal* 874.1 (2019), p. 4 (cit. on p. 58).